Locked modes precursors from the electron temperature profile in plasma termination on JET

Presented by Gianluca Pucella

ENEA, Fusion and Nuclear Safety Department, C.R. Frascati, Italy

This work has been carried out within the framework of the EUROfusion Consortium, funded by the European Union via the Euratom Research and Training Programme (Grant Agreement No 101052200 — EUROfusion). Views and opinions expressed are however those of the author(s) only and do not necessarily reflect those of the European Union or the European Commission. Neither the European Union nor the European Commission can be held responsible for them.

Acknowledgements

With thanks to my co-authors:

E. Alessi[2], F. Auriemma[3], M. Baruzzo[1], D. Brunetti[4], P. Buratti[5], C.D. Challis[4], A. Chomiczewska[6], E. De La Luna[7], D.R. Ferreira[8], M. Fontana[4], D. Frigione[5], L. Garzotti[4], E. Giovannozzi[1], J. Hobirk[9], E. Joffrin[10], A. Kappatou[9], E. Lerche[11], P.J. Lomas[4], S. Nowak[2], A. Pau[12], L. Piron[13], F. Rimini[4], C. Sozzi[2], D. Van Eester[11] and JET Contributors*

[1] ENEA, Fusion and Nuclear Safety Department, C.R. Frascati, Italy
[2] ISTP, Consiglio Nazionale delle Ricerche, Milano, Italy
[3] Consorzio RFX, Padova, Italy
[4] UKAEA, Culham Science Centre, Abingdon, UK
[5] Università degli Studi di Roma "Tor Vergata", Roma, Italy
[6] Institute of Plasma Physics and Laser Microfusion, Warsaw, Poland
[7] CIEMAT, Laboratorio Nacional de Fusión, Madrid, Spain
[8] IPFN/IST, University of Lisbon, Lisbon, Portugal
[9] Max-Planck-Institut für Plasmaphysik, Garching, Germany
[10] CEA, IRFM, Saint-Paul-lez-Durance, France
[11] Laboratory for Plasma Physics, ERM/KMS, Brussels, Belgium
[12] EPFL, Swiss Plasma Centre, Lausanne, Switzerland
[13] Università degli Studi di Padova, Padova, Italy

*See the author list of J Mailloux et al. 2022 Nucl. Fusion https://doi.org/10.1088/1741-4326/ac47b4

Outline

Plasma disruptions

- Operation safety & scenario development
- Disruption prevention & emergency shutdown
- Data-driven & physics-driven models for disruption prediction

Tearing modes in plasma termination on JET

- Experimental observations
- The role of current density gradient
- Interpretative TRANSP simulations
- Linear stability analysis in toroidal geometry

Temperature hollowing and edge cooling

- Parameters characterizing the shape of Te profile
- Empirical stability diagram
- Characteristic time scales
- Locked modes precursors for avoidance & mitigation actions

Plasma disruptions

- The capability to carried out plasma pulses safely is an important goal towards the optimization of an operating scenario:

Disruption
- safety → thermal loads, electromagnetic loads, formation and impact of runaway electrons
- scenario → limits to the range of accessible plasma parameters

Prevention & shutdown
- disruption prevention → plasma control throughout the entire evolution of the pulse (break down in different “control phases”)
- emergency shutdown → terminate the pulse in a controlled way or alleviate the consequences of unavoidable disruptions

Disruption prevention & emergency shutdown

- **Disruption prevention** is a multi-stage approach covering the full range of control regimes to prevent the disruption; **emergency shutdown** involves the anticipated termination of a pulse.

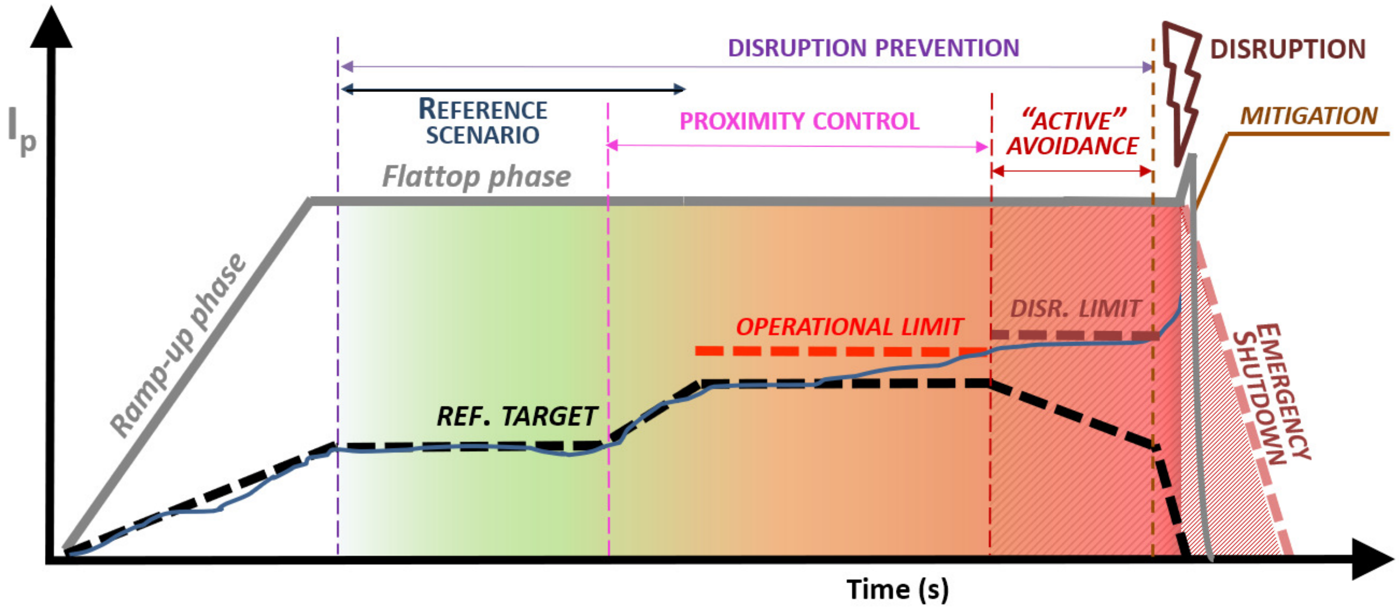

[A. Pau, EPS 2022]

"Disruption-free protocol" (ITPA- IOS)

REFERENCE SCENARIO	PROXIMITY CONTROL	ACTIVE AVOIDANCE	EMERGENCY SHUTDOWN
Keep the target scenario stable again disturbances (ST, ELM, MHD modes, etc.)	Keep stability while pushing performance by regulating proximity to stability & controllability boundaries	Asynchronous response when crossing operational boundaries (danger levels)	• Fast controlled shutdown • Mitigation

Disruption prediction

- **Data-driven models** derived from machine learning methods, with high accuracy levels (success rate of above 95 %, false alarms rate of few %):
  - Supervised learning: training dataset, allowing the model to learn over time
  - Unsupervised learning: unlabeled data, helping to discover hidden patterns or data clustering

ML references →

- **Physics-driven models** based on physics understanding of the phenomenon involved in a particular class of disruptions:
  - results easier to interpret in terms of plasma dynamics
  - large amount of data for training is not required

Case study →

Machine Learning for disruption prediction

- Remarkable success in data-driven models for disruption identification and real-time control, including high-performance work models not limited to a specific device.

Neural Networks

B. Cannas et al 2007 A prediction tool for real-time application in the disruption prediction system at JET Nucl. Fusion **47** 1559

R. Yoshino et al 2003 Neural-net disruption predictor in JT-60U Nucl. Fusion **43** 1771

Mapping and Manifold Learning

B. Cannas et al 2014 Overview of manifold learning techniques for the investigation of disruptions on JET Plasma Phys. Control. Fusion **56** 114005

A. Pau et al 2019 A machine learning approach based on generative topographic mapping for disruption prevention and avoidance at JET Nucl. Fusion **59** 106017

Decision Tree, CART, Random Forest, GBM

K.J. Montes et al 2019 Machine learning for disruption warnings on Alcator C-Mod, DIII-D, and EAST Nucl. Fusion **59** 096015

A. Murari et al 2020 On the transfer of adaptive predictors between different devices for both mitigation and prevention of disruptions, Nucl. Fusion **60** 056003

Support Vector Machines

J. Vega et al 2013 Results of the JET real-time disruption predictor in the ITER-like wall campaigns, Fusion Eng. Des. **88** 1228

G. Rattá et al 2010 An advanced disruption predictor for JET tested in a simulated real-time environment, Nucl. Fusion **50** 025005

Statistical Learning

Y. Zhang, G. Pautasso et al 2011 Prediction of disruptions on ASDEX Upgrade using discriminant analysis, Nucl. Fusion **51** 063039

S.P. Gerhardt et al 2013 Detection of disruptions in the high-β spherical torus NSTX Nucl. Fusion **53** 063021

Deep Learning

J. Kates-Harbeck, A. Svyatkovskiy and W. Tang 2019 Predicting disruptive instabilities in controlled fusion plasmas through deep learning Nature **568** 526

J.X. Zhu et al 2021 Hybrid deep-learning architecture for general disruption prediction across multiple tokamaks Nucl. Fusion **61** 026007

Current ramp-up of the hybrid scenario at JET

- **Physics understanding**: double tearing modes in pulses with hollow Te-profiles [C.D. Challis, Nucl. Fusion 2020]

↓

Slower current ramp-up and higher density led to a stable scenario (**reference scenario**)

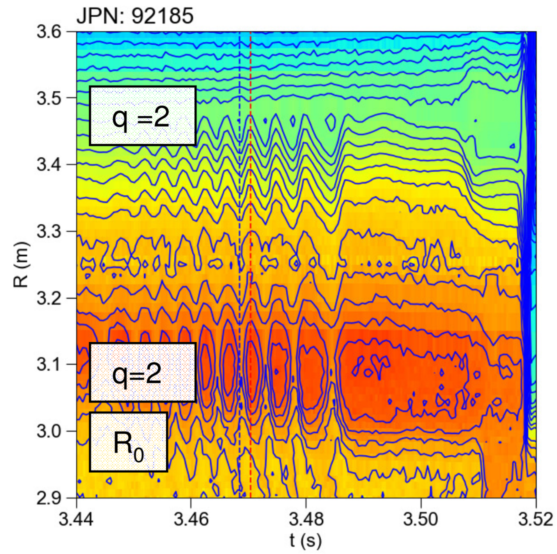

[G. Pucella, to be submitted]

Te-profile peaking factor [M. Fontana FED 2020] included in the **JET RT control system** [L. Piron FED 2021]

active avoidance →
- Central heating
- Density control

emergency shutdown →
- Early pulse termination (implemented)

JET MGI system, based on locked mode signals, can be triggered (**mitigation**)

Tearing modes in plasma termination on JET

- **Tearing modes** in the termination phase of pulses with anomalous Te-profiles

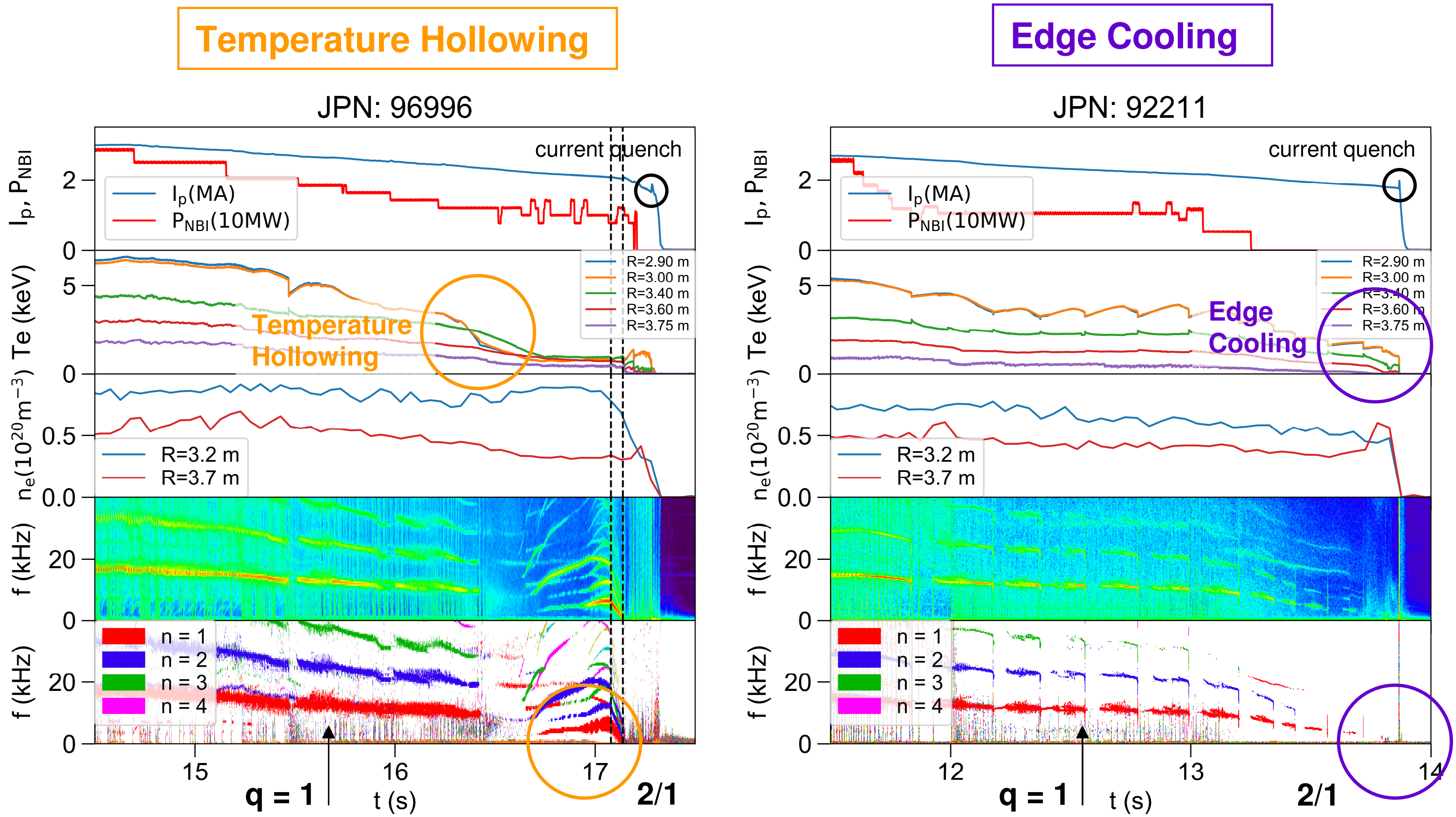

[G. Pucella et al. Nucl. Fusion 2021]

Termination phase: radiation emission and Te profiles

Temperature Hollowing

JPN: 96996

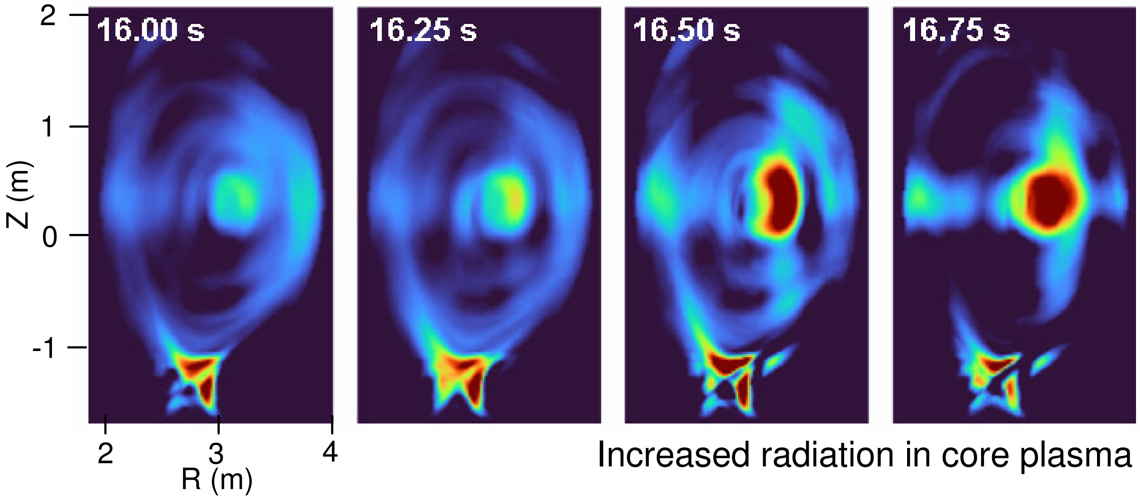

Increased radiation in core plasma

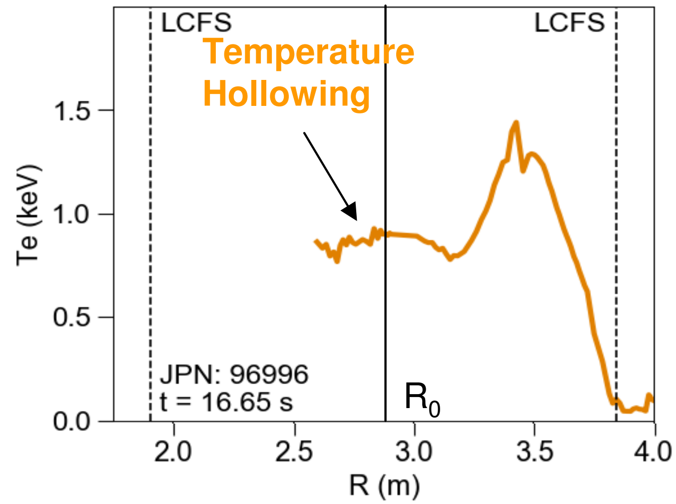

Bolometer data

Edge Cooling

JPN: 92211

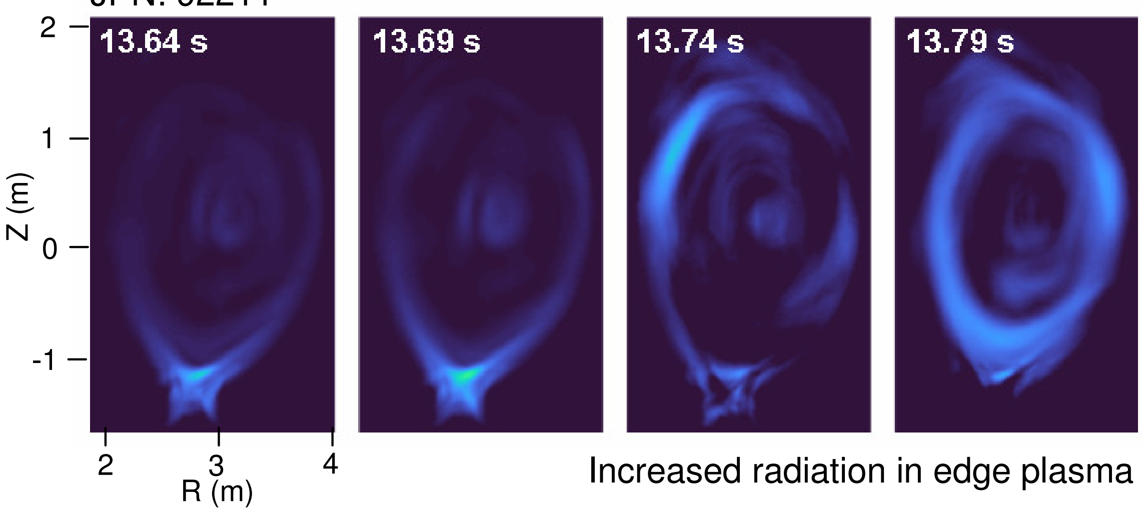

Increased radiation in edge plasma

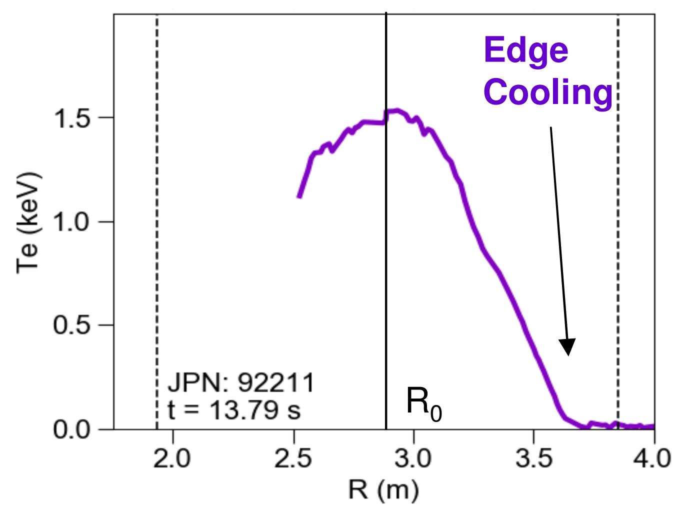

Temperature Hollowing: MHD activity

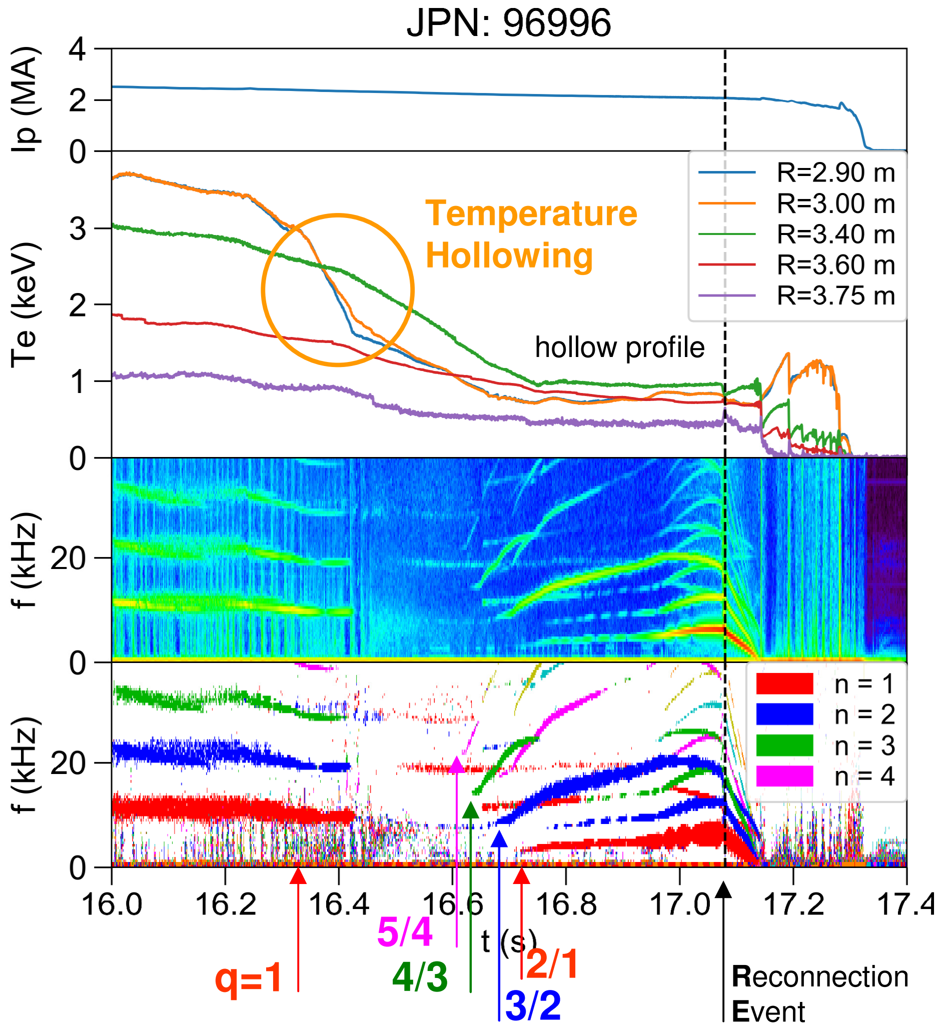

- Hollowing of Te profile
- Disappearance of q = 1 activity
- Sequence of modes with decreasing **n**

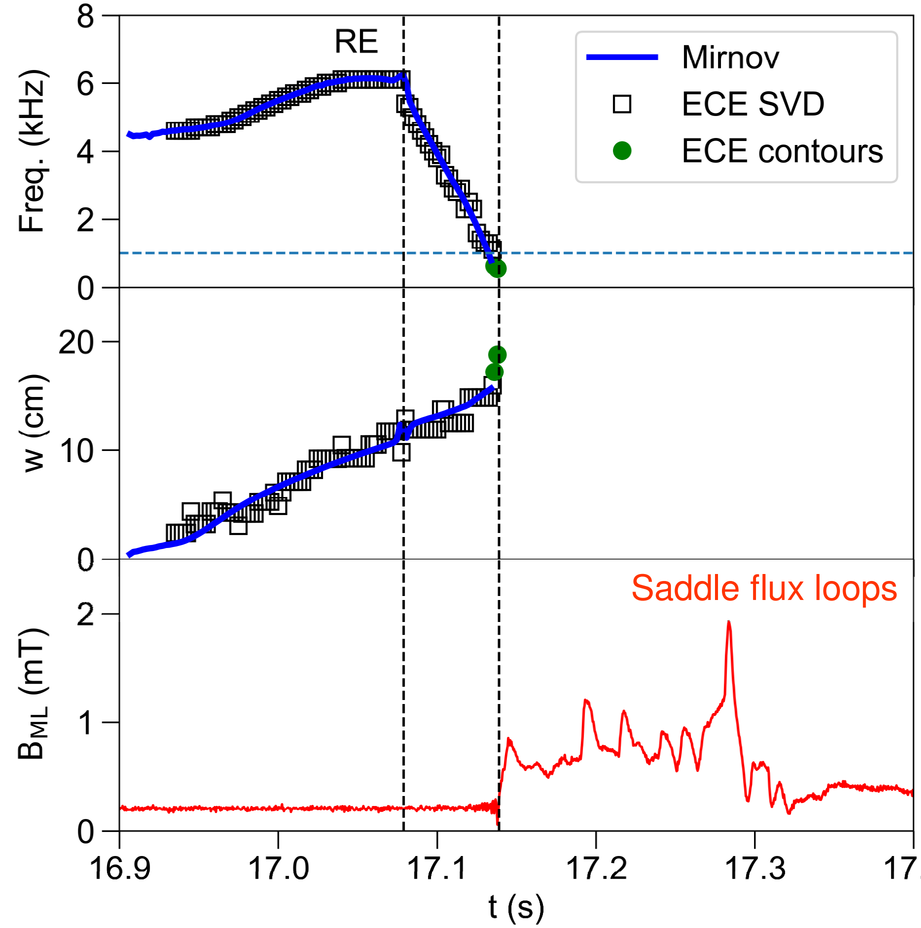

2/1 mode characterized by a fast initial mode rotation

Edge Cooling: MHD activity

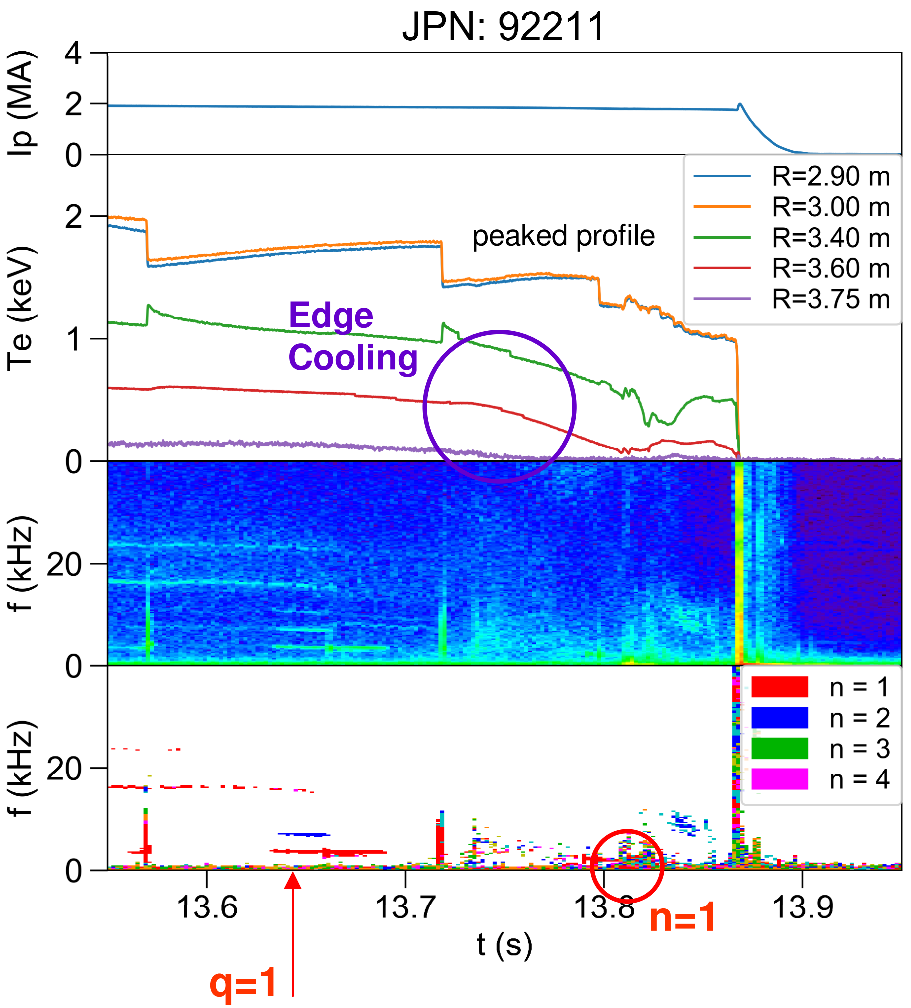

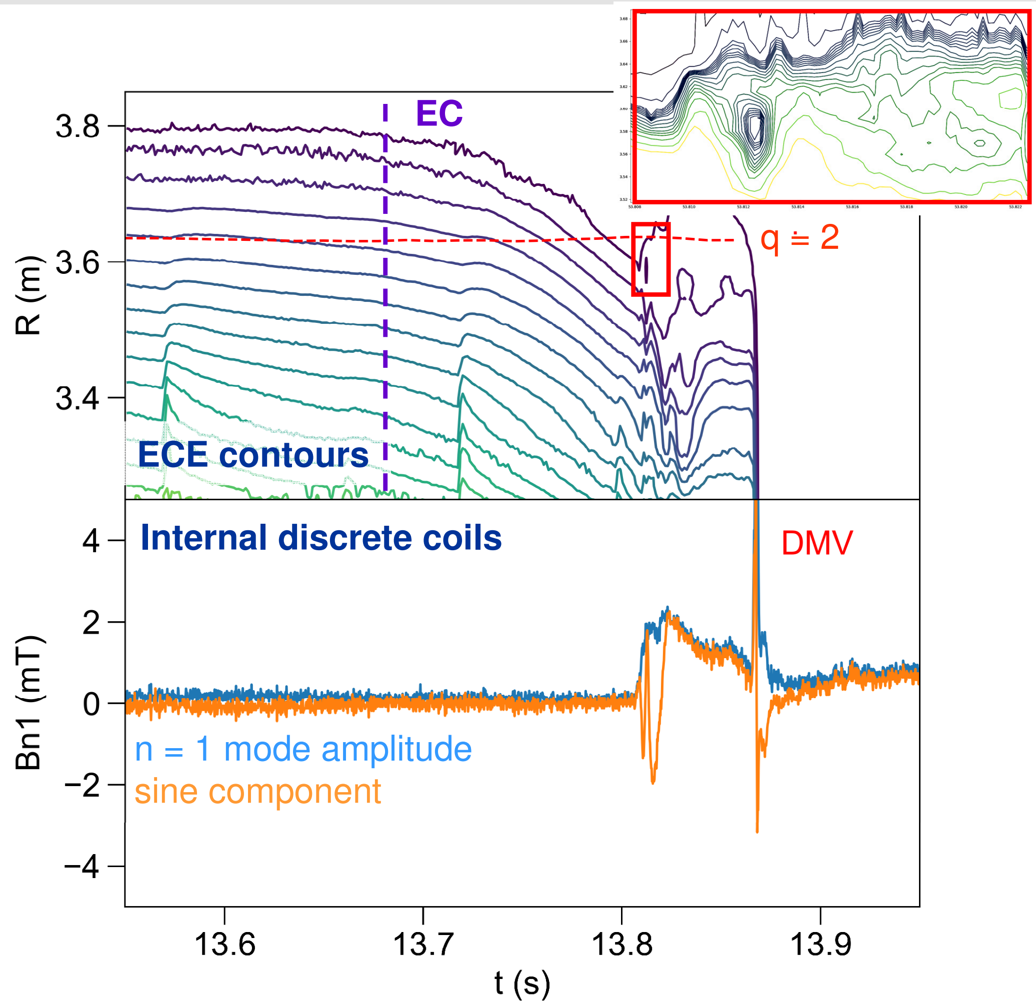

- Peaked Te-profile
- Increasing variations on ECE contours near the q = 2 surface

2/1 mode usually makes only a few turns before locking

Destabilization mechanism

- Tearing mode destabilization driven by the radial gradient of the current density profile:

$$\frac{d}{dr}\left[\left\langle\frac{g_{\theta\theta}}{\sqrt{g}}\right\rangle\frac{d}{dr}\left(rB_{r1}\right)\right]=\left[\left\langle\frac{g_{rr}}{\sqrt{g}}\right\rangle m^2+\frac{\mu_0 q}{\left(1-nq/m\right)}\frac{d}{dr}\left\langle\frac{j_{tor}}{B_{tor}}\right\rangle\right]\left(rB_{r1}\right)$$

zero pressure limit

Cylindrical limit:

$g_{rr}=1\,;\ g_{\theta\theta}=r^2\,;\ g_{\phi\phi}=R_0^2$

$\sqrt{g}=rR_0$

  - Current profile dominated by the ohmic contribution in the termination phase and **high resistivity** due to low temperature:

$$\eta\propto Z_{eff}/T_e^{3/2}$$

  - Current profile changing on a relatively **short resistive diffusion time scale** reflecting the changes in the electron temperature profile:

$$\tau_R\approx\mu_0 L^2/\eta$$

  - Possibility of **2/1 tearing modes linearly destabilized** by changes in the current density profile.

Broadening and shrinking of current density profile

Edge Cooling and **Temperature hollowing** can destabilize a 2/1 tearing mode as a consequence of J-profile changes:

- **shrinking** in case of edge cooling
- **broadening** in case of temperature hollowing

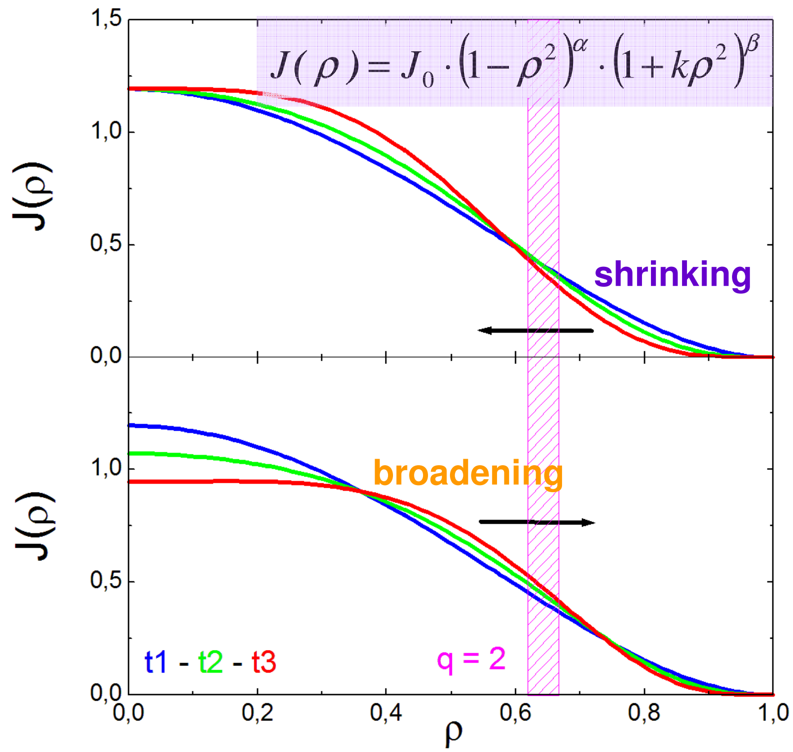

Open questions

- Is the current density profile changing before the mode onset ? → TRANSP simulations
- Do profile changes lead to an unstable scenario ? → Linear stability analysis

TRANSP simulations

- Interpretative TRANSP simulations carried out for the two pulses mentioned before: **JPN 96996** (**temperature hollowing**) and **JPN 92211** (**edge cooling**).

  Te & ne: high-resolution TS ; Ti = Te ; J: poloidal field equation solved ; η: Spitzer

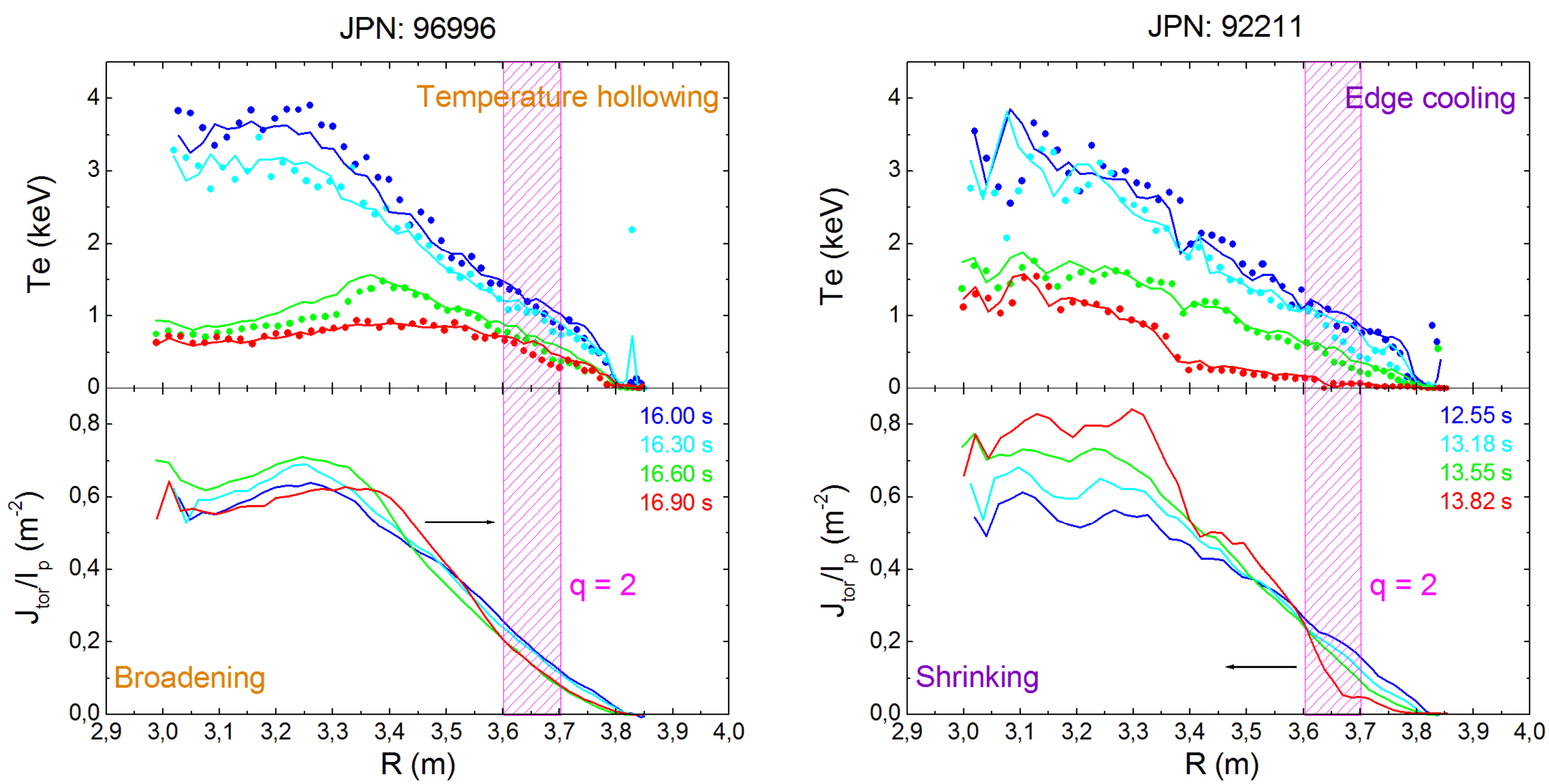

Stored energy and total neutrons within 10% of experimental values

- Changes in J-profile reflecting changes in Te-profile
  Delay between Te and J profiles: **500 ms** (JPN 96996), **100 ms** (JPN 92211)

Linear stability analysis

- Linear stability criterion in the zero pressure approximation:

$$\Delta' \equiv \left.\frac{d\,\ln B_{r1}}{dr}\right|_{s+} - \left.\frac{d\,\ln B_{r1}}{dr}\right|_{s-} \propto -\delta W_{mag} \quad ; \quad \Delta' < 0 \xrightarrow{pressure,\ \ curvature} \Delta' < K(\beta, 1/\eta)$$

Jump across the mode resonant surface

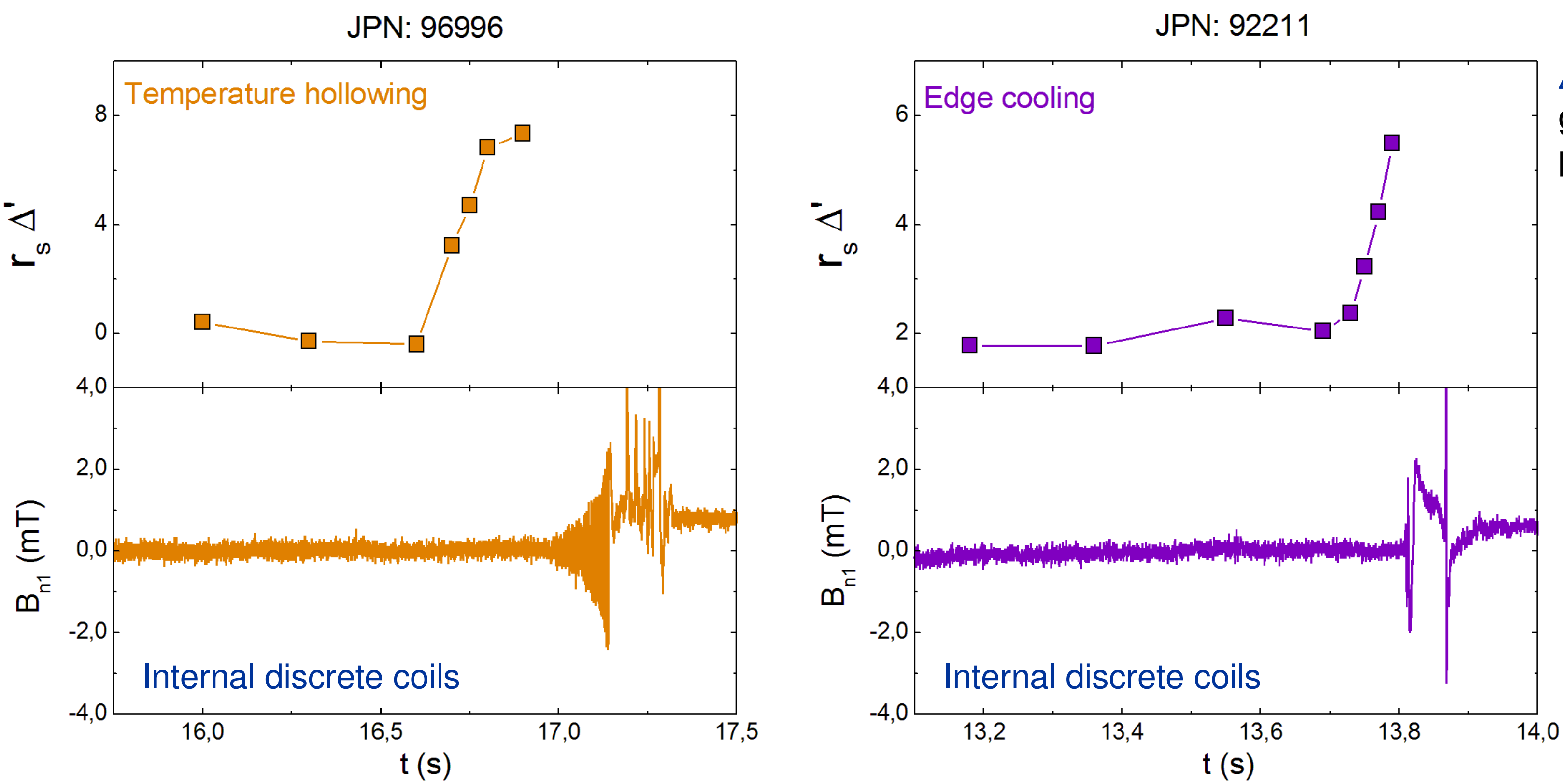

Δ' calculated in toroidal geometry neglecting pressure effects

Δ' increasing
K decreasing → destabilization process

Recurrent paths

- Paths leading to the onset of 2/1 tearing modes:
  - Core accumulation of high-Z impurities → Temperature Hollowing → j_ϕ broadening
  - Influx of low-Z impurities → Edge Cooling → j_ϕ shrinking

Outboard radiating blob due to high-Z impurities in the LFS ⇢ Edge Cooling

2/1 TM destabilization
(Δ' increase)

Temperature Hollowing

Edge Cooling

Spontaneous onset

Reconnection event

Hollowing, but final collapse from edge

Onset with peaked temperature profile

j_ϕ broadening

j_ϕ shrinking

Temperature hollowing and edge cooling parameters

Temperature Hollowing	**Edge cooling**	
$TH \equiv \frac{\langle Te \rangle_{Vmid}}{\langle Te \rangle_{Vint}}$	$EC \equiv \frac{\langle Te \rangle_{Vmid}}{\langle Te \rangle_{Vext}}$	V_{int} R = 3.00 - 3.40 m V_{mid} R = 3.40 - 3.60 m V_{ext} R = 3.60 - 3.75 m

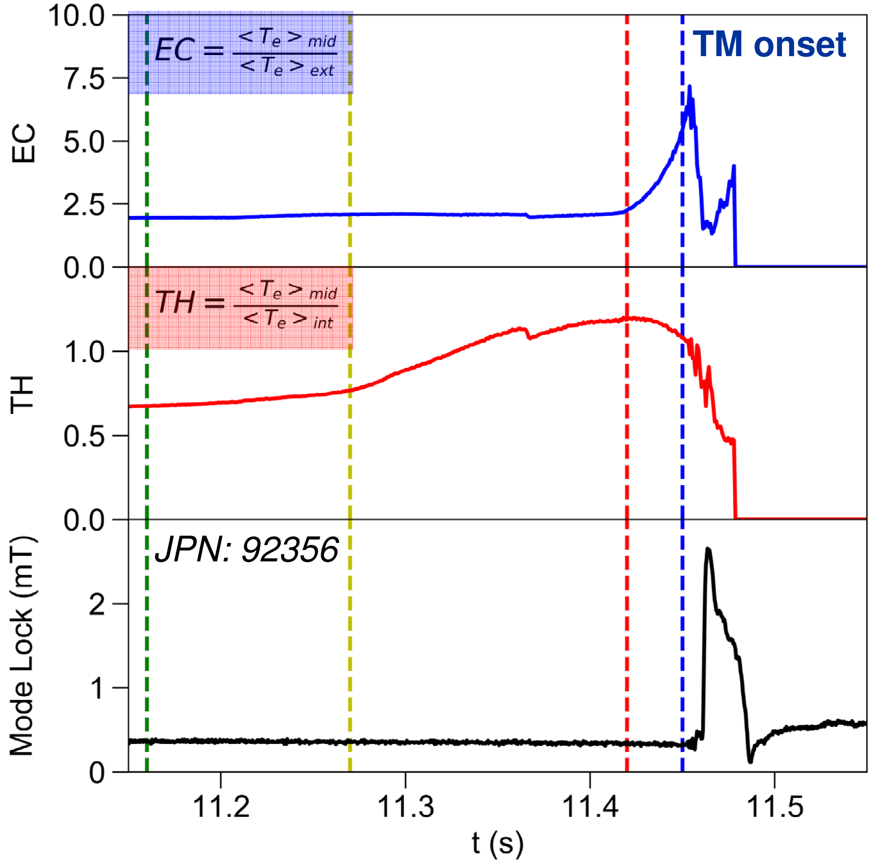

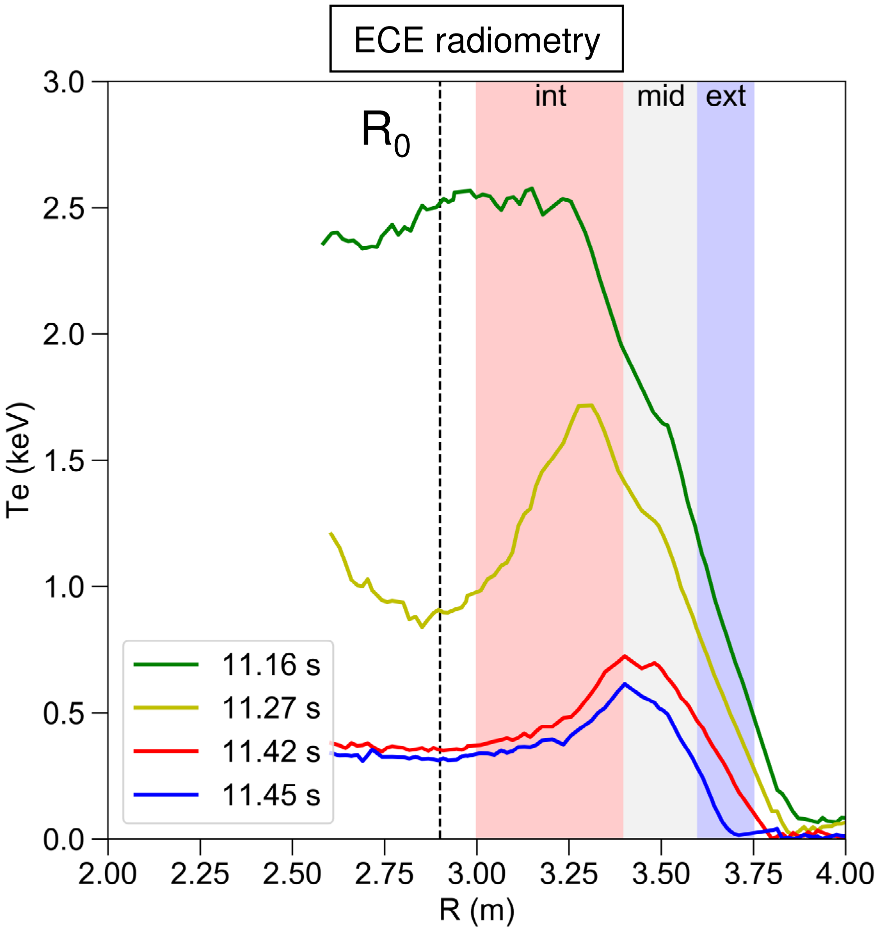

Temperature hollowing and edge cooling parameters

- TH and EC parameters for the two pulses mentioned before:

  JPN 96996 - temperature hollowing
  JPN 92211 - edge cooling

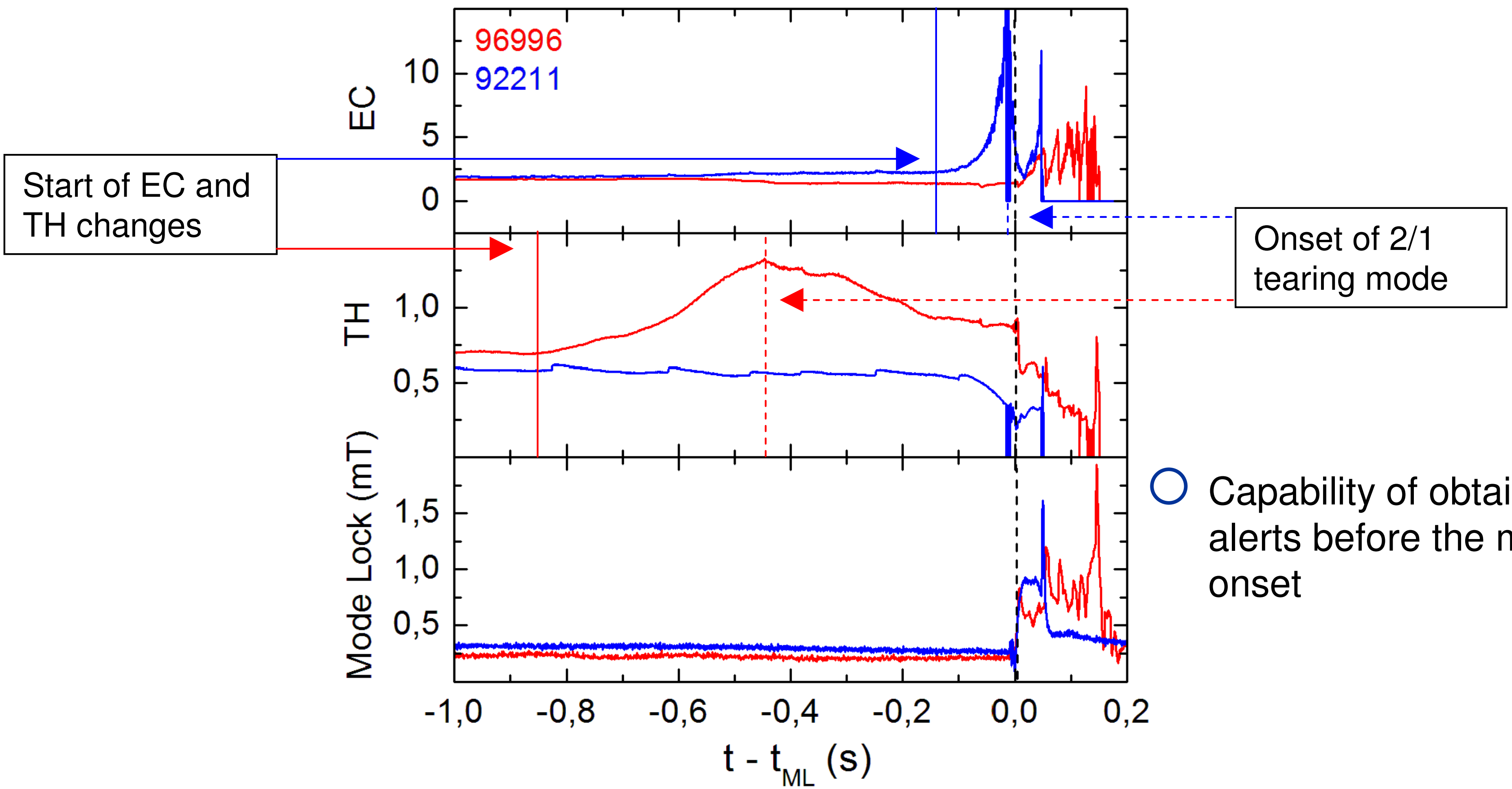

- Capability of obtaining alerts before the mode onset

Non-disruptive and disruptive pulses

- Dataset of 268 pulses: 136 non-disruptive, 132 disruptive
  Baseline scenario: Ip = 2.5 - 3.7 MA

Non-disruptive pulses

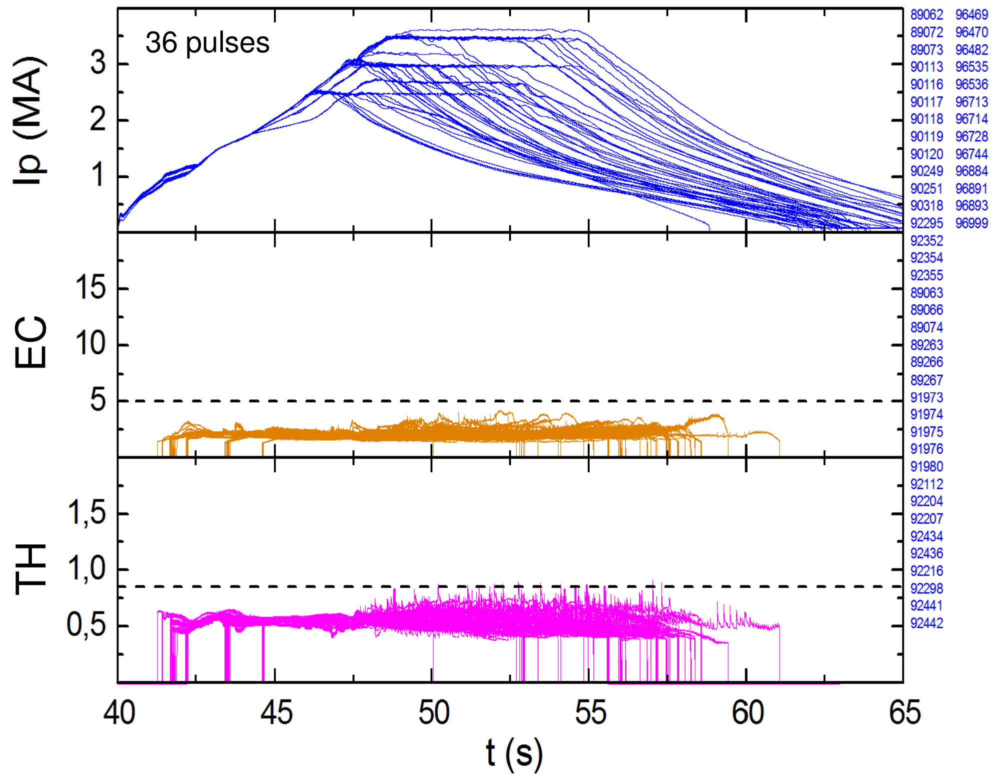

Disruptive pulses

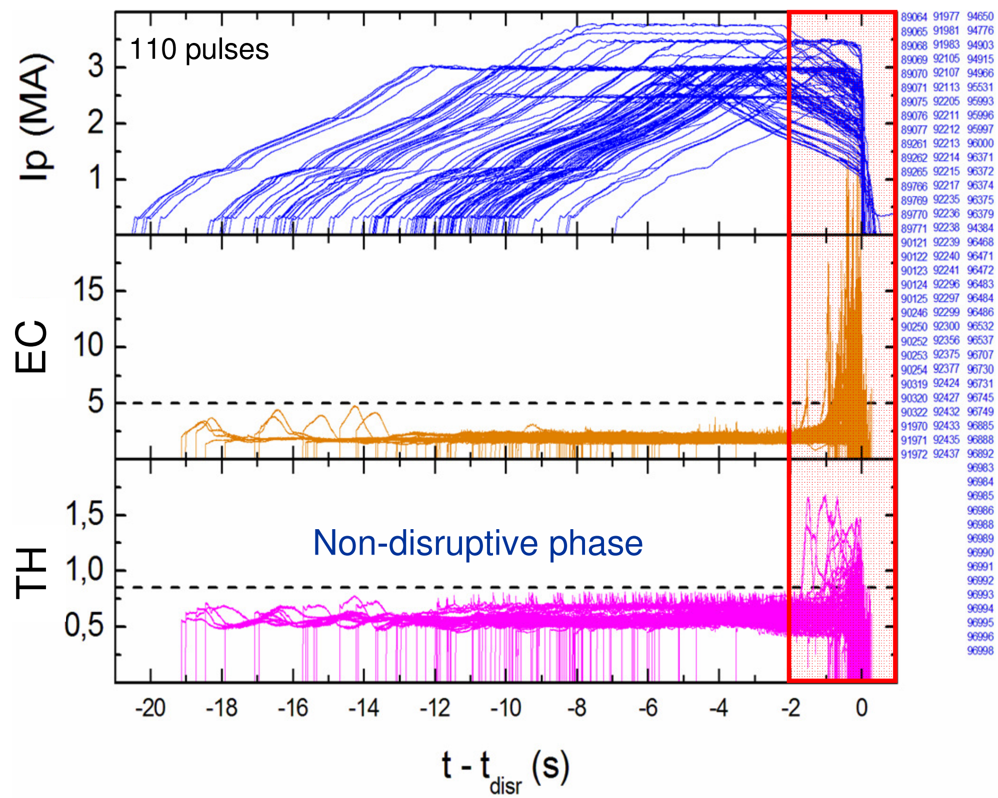

- Stable values for TH and EC (10% false positive)
- TH, EC increase in the last **2 s** before disruption (90% right alerts)

Empirical stability diagram

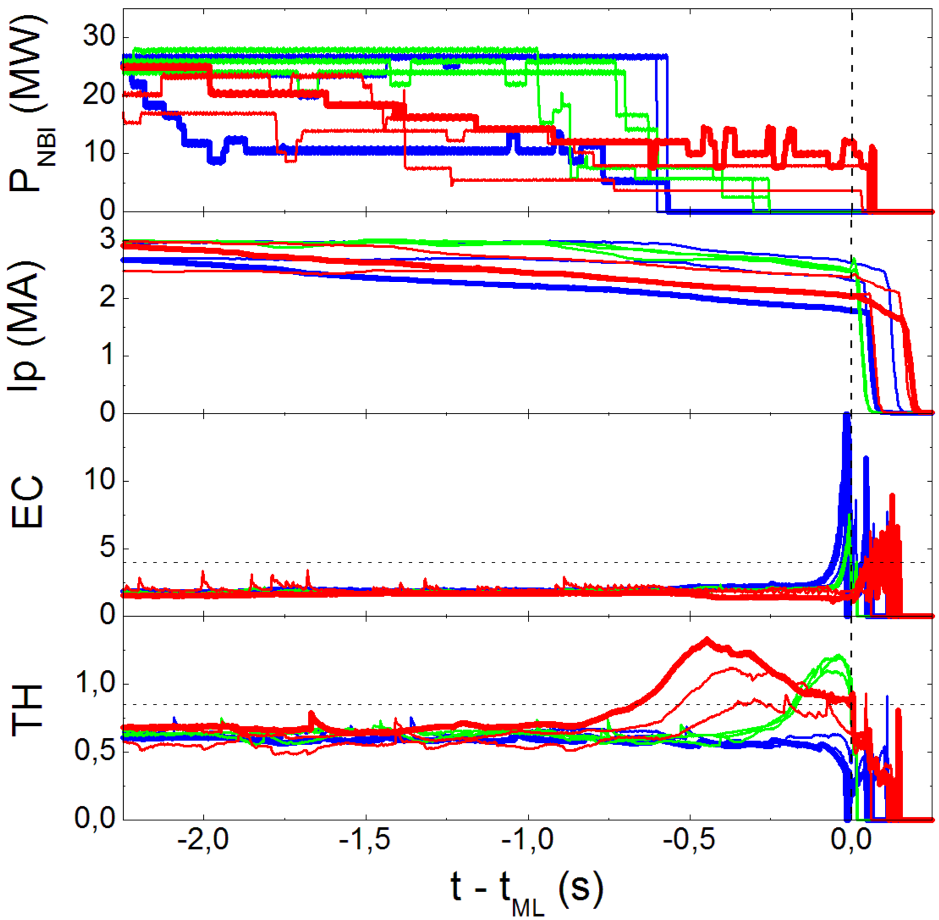

Paths of representative pulses on the (EC-TH) plane

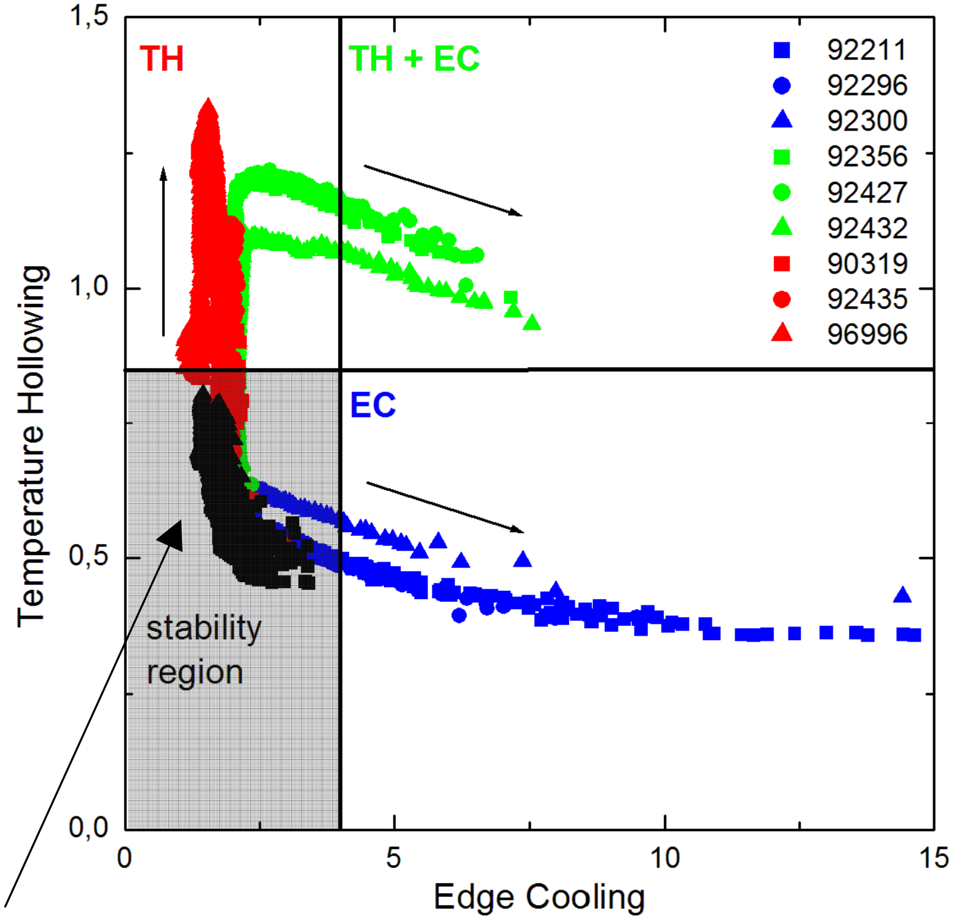

(EC-TH) pairs between
5s and 1s to ML

Characteristic time scales: mode locking and disruption

- Mode locking used as a reference for the evaluation of characteristic time scales

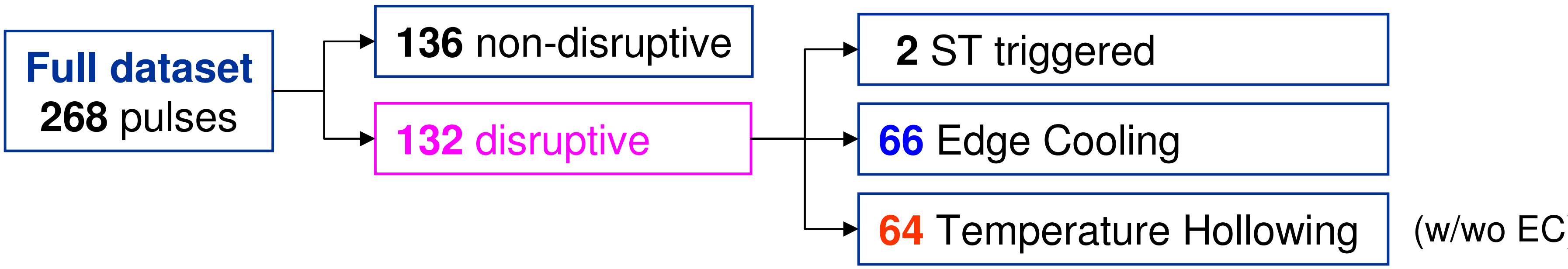

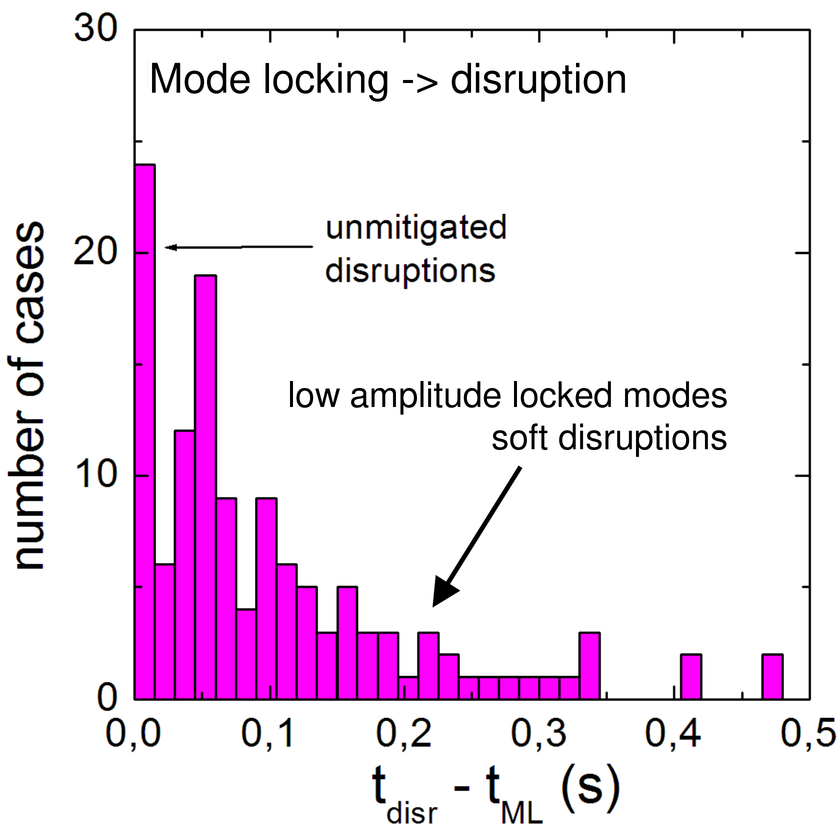

- Time from mode locking to disruption depending on mode dynamics and DMV logic

Characteristic time scales: TH and EC

- Distributions of the time interval between the increase of **EC** and **TH** and the **mode locking**

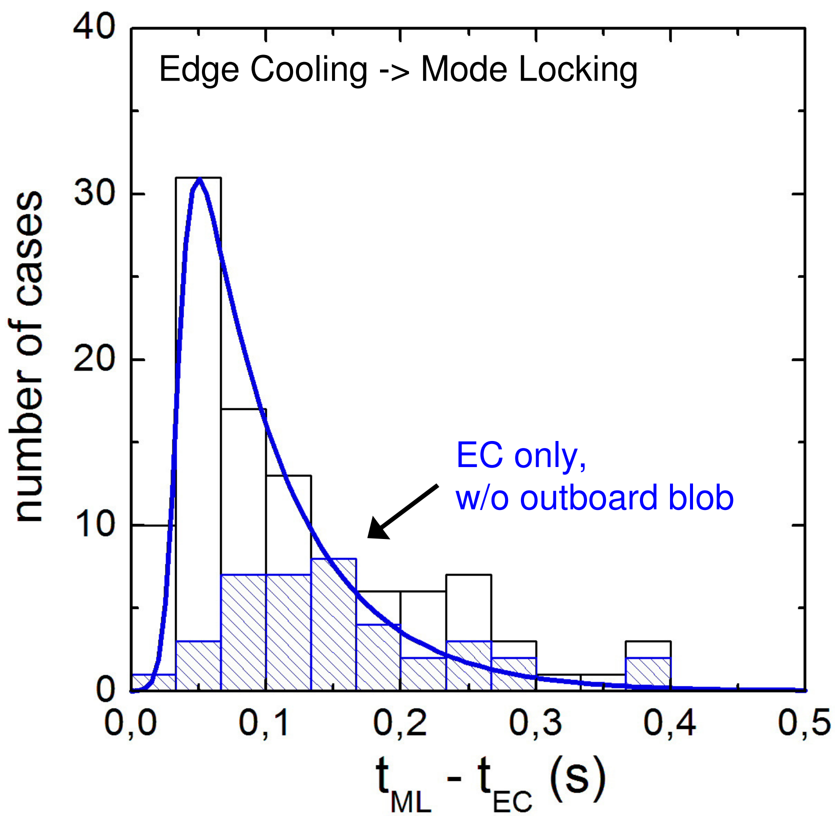

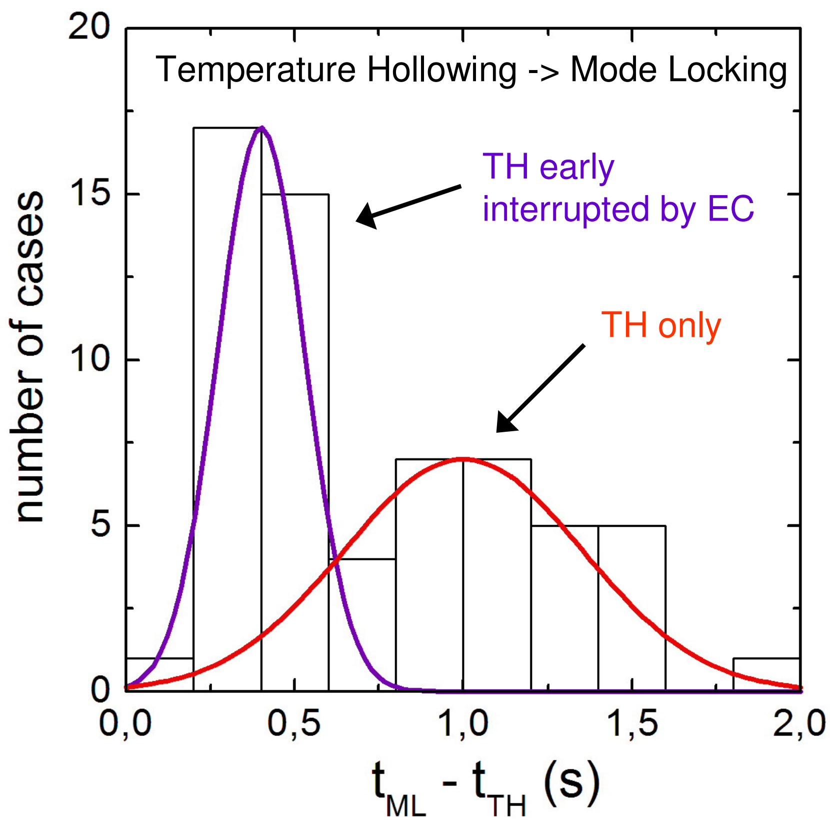

- **EC** could provide alerts within **200 ms** from the ML: sufficient to anticipate **mitigation** actions

- **TH** could provide alerts up to **2 s** from the ML: an attempt to **avoid** the disruption is possible

Avoidance actions

- **Central additional heating** to counteract the inward transport of high-Z impurities in case of **temperature hollowing**

  Additional power to be calibrated to avoid the onset of TM triggered by long-period ST-crashes

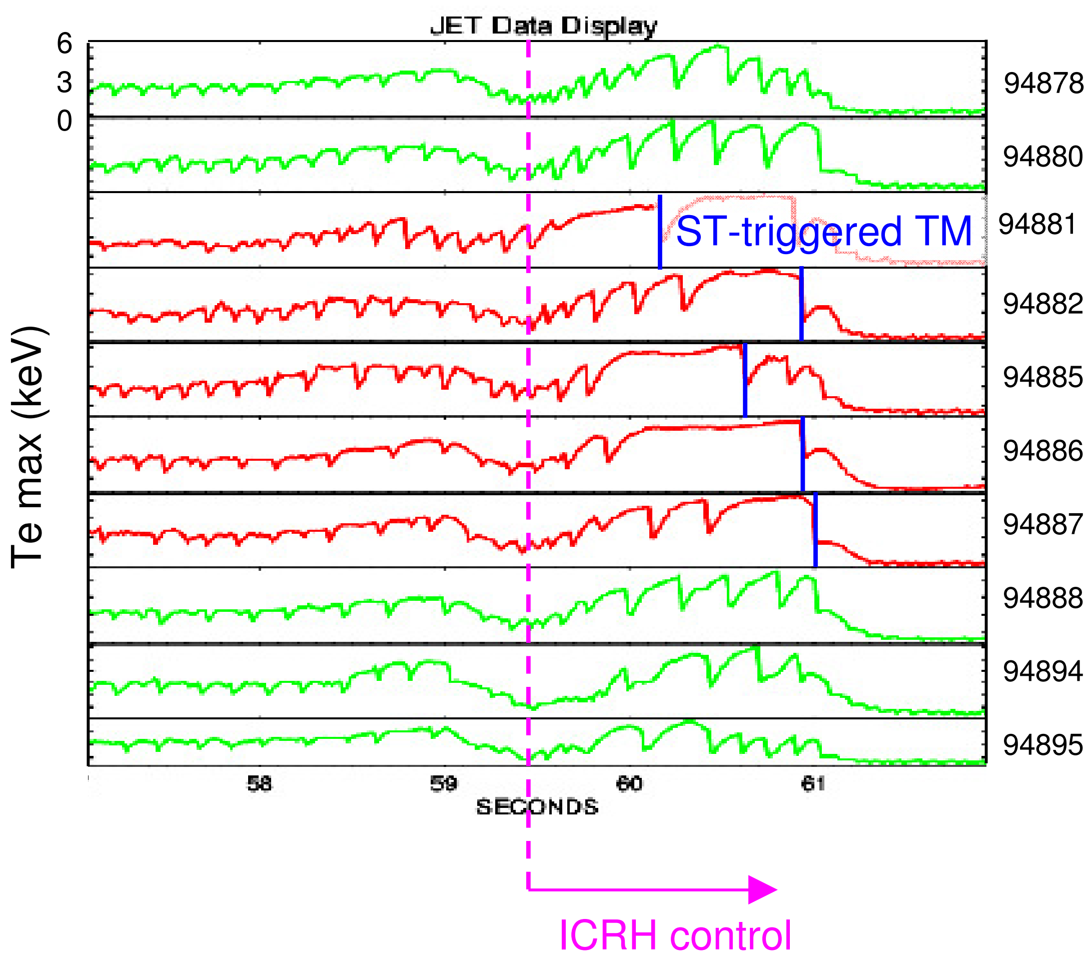

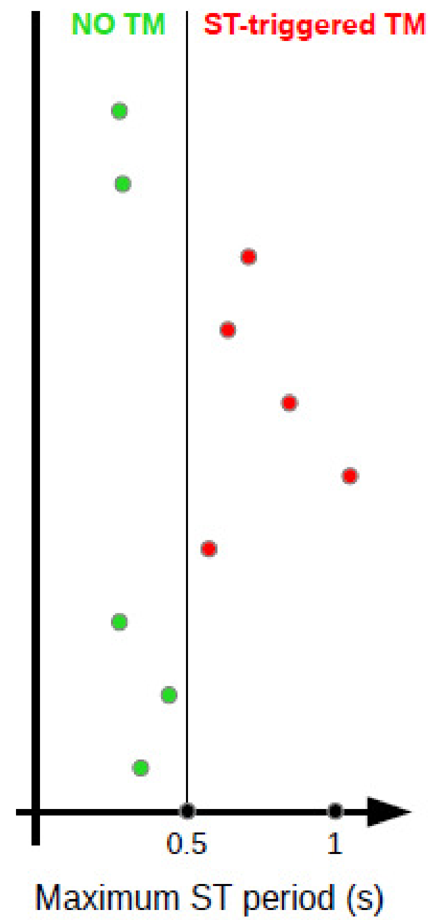

Mitigation actions

- **Gas injection**, leading to a fast loss of thermal energy by photon radiation, in case of **edge cooling**
  - Mode saturation for EC in **peaked Te profile**
    Thermal quench is induced by DMV intervention → not crucial to anticipate DMV
  - Explosive growth for EC in **hollow Te profile**
    Some unmitigated thermal quenches → crucial to anticipate DMV

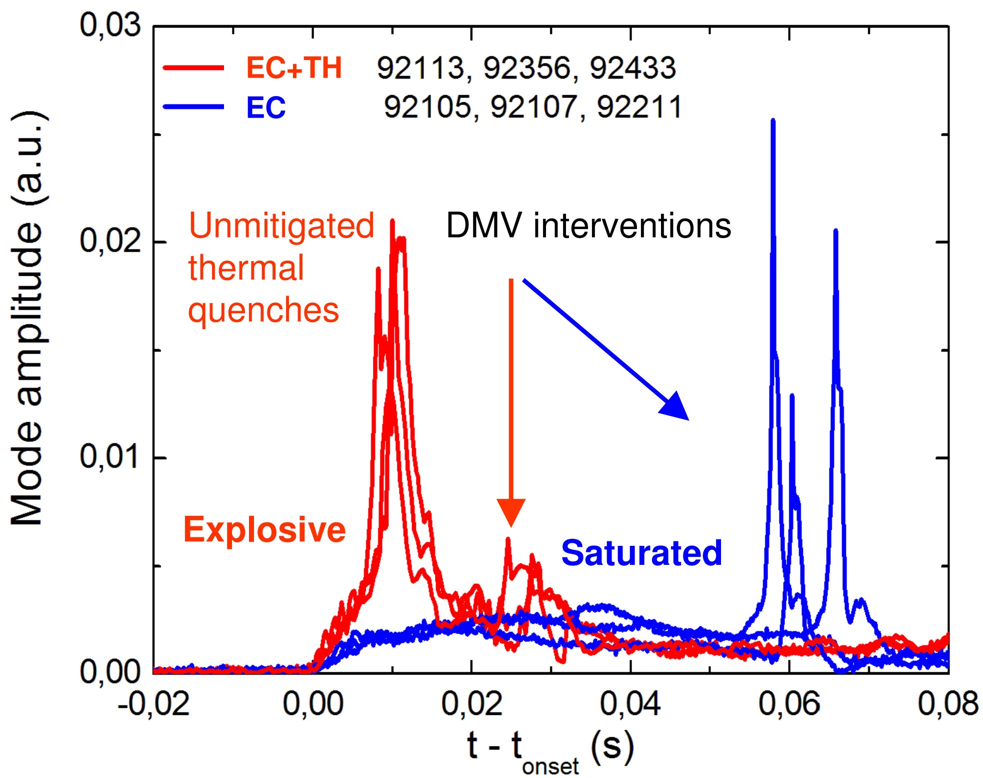

- More detailed analysis of the explosive growth in view of ITER

Conclusions

- Tearing modes in the termination phase of JET pulses in presence of an increased radiation emission in core or edge plasma, leading to **temperature hollowing** and **edge cooling**

- Both cases can lead to the linear destabilization of a 2/1 TM: **J-broadening** in case of temperature hollowing, **J-shrinking** in case of edge cooling

- Two parameters defined to highlight temperature hollowing (**TH**) and edge cooling (**EC**), confirming that changes in Te-profile described by the two parameters strongly increases the risk of destabilizing a 2/1 TM

- **Locked mode precursors** based on TH & EC: TH could provide alerts (~ **1 s**) useful for avoidance actions; EC could provide alerts (~ **100 ms**) useful to anticipate mitigation actions

- Additional information by the dynamics of n=1 mode signals, highlighting explosive modes to be studied in view of ITER

TRANSP setting

Equilibrium: EFIT
q: poloidal field equation solved
AF: no rotation provided
NE, TE: HRTS
TI = TE

ZEFF: ZEFH flat profile
PRAD: BOLP/TOBP flat profile
Impurity: Be only
η: Spitzer

JPN 96996 – Temperature Hollowing

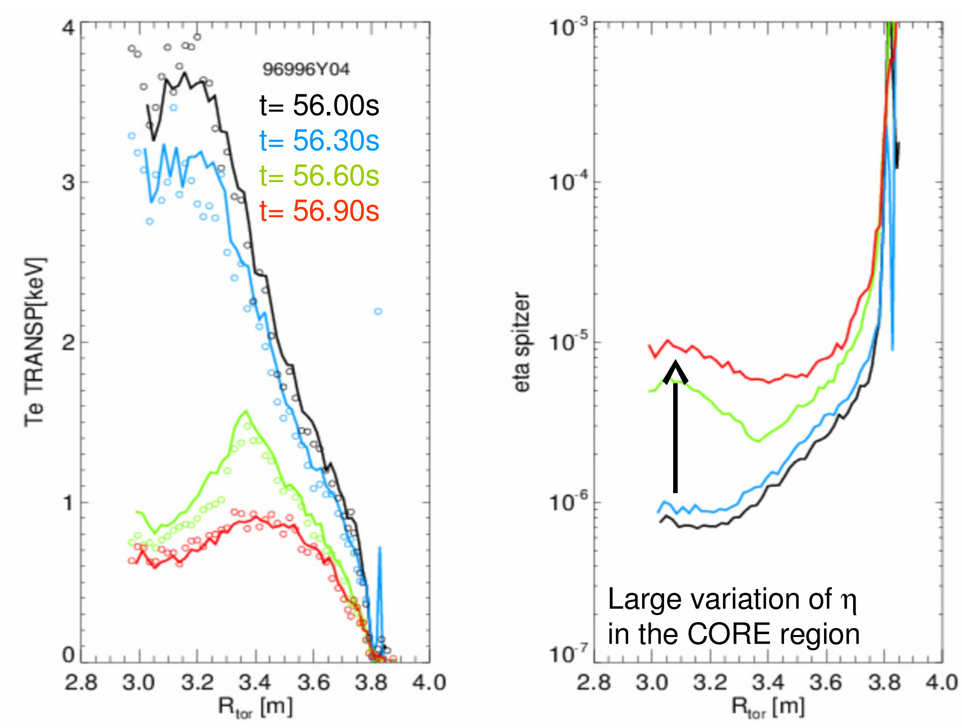

JPN 92211 – Edge Cooling

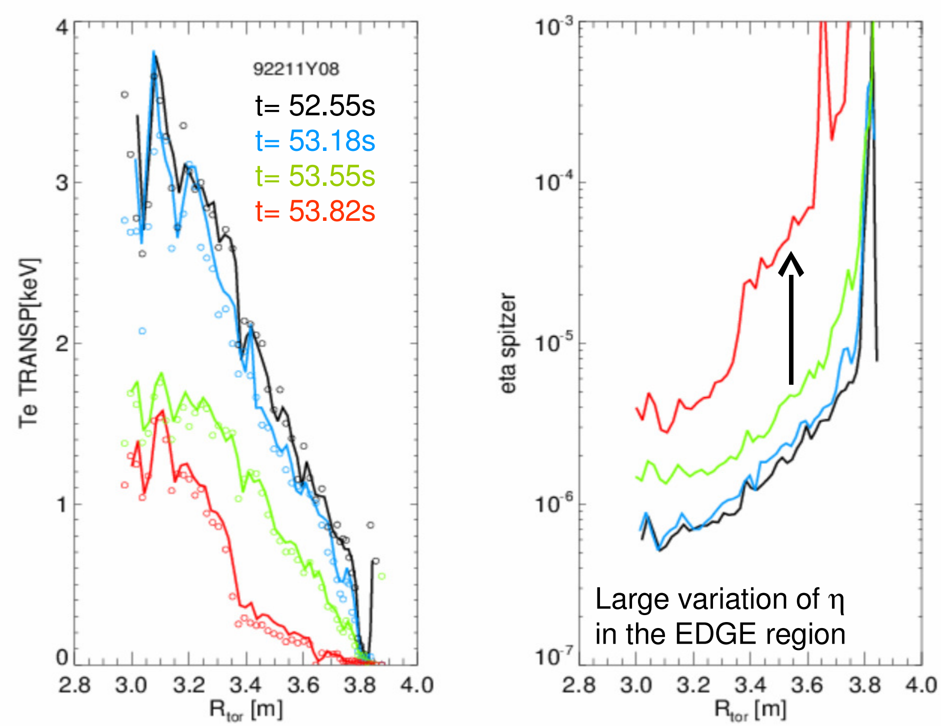

Linear stability analysis

- Linear stability criterion in the zero pressure approximation:

$$\Delta' \equiv \left.\frac{d\,\ln B_{r1}}{dr}\right|_{s+} - \left.\frac{d\,\ln B_{r1}}{dr}\right|_{s-} \propto -\delta W_{mag} \quad ; \quad \Delta' < 0 \xrightarrow{pressure,\ \ curvature} \Delta' < K(\beta, 1/\eta)$$

Jump across the mode resonant surface

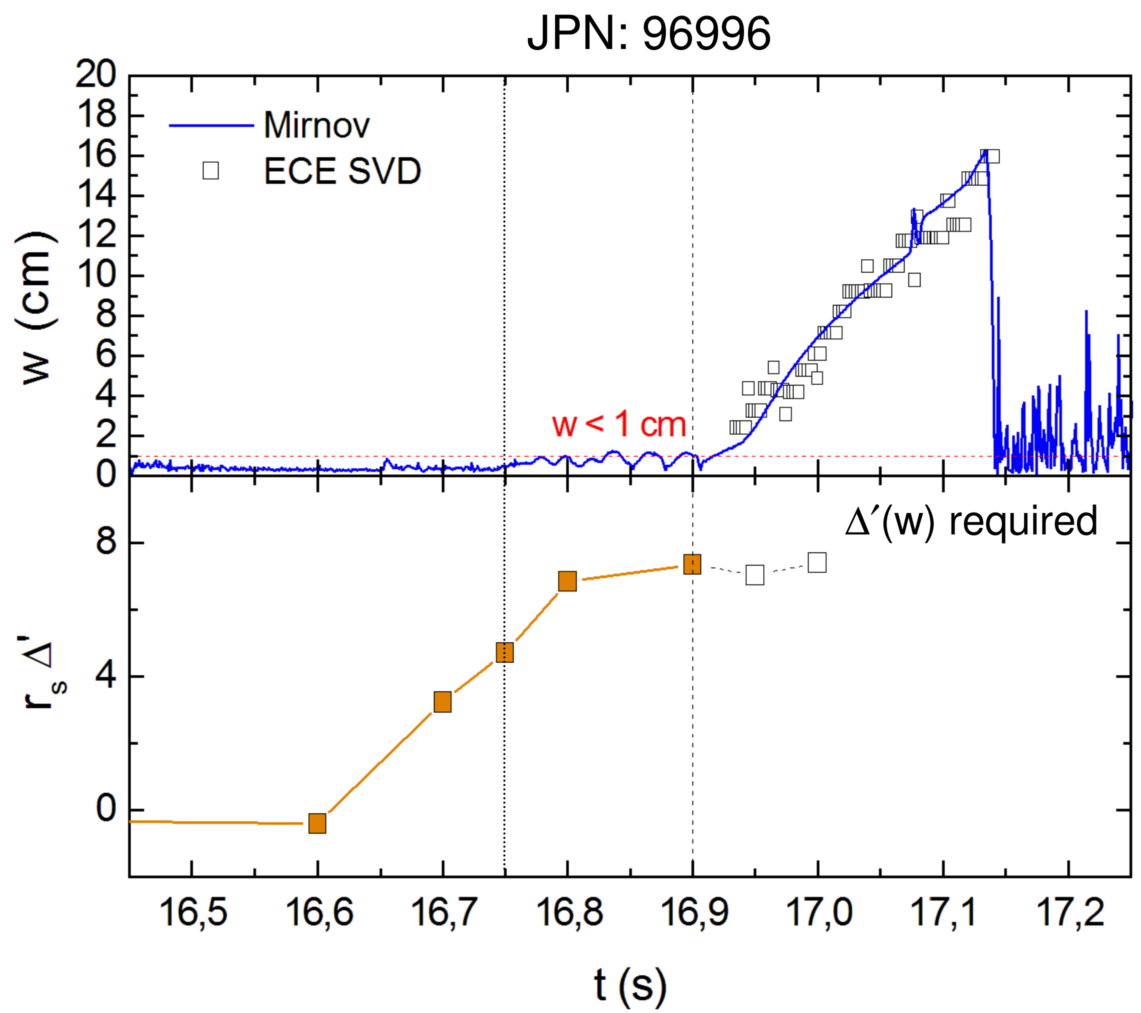

Sequence of mode onsets

- A sequence of mode onsets with decreasing toroidal mode number n is observed in pulses with progressive temperature hollowing: 5/4 -> 4/3 -> 3/2 -> 2/1

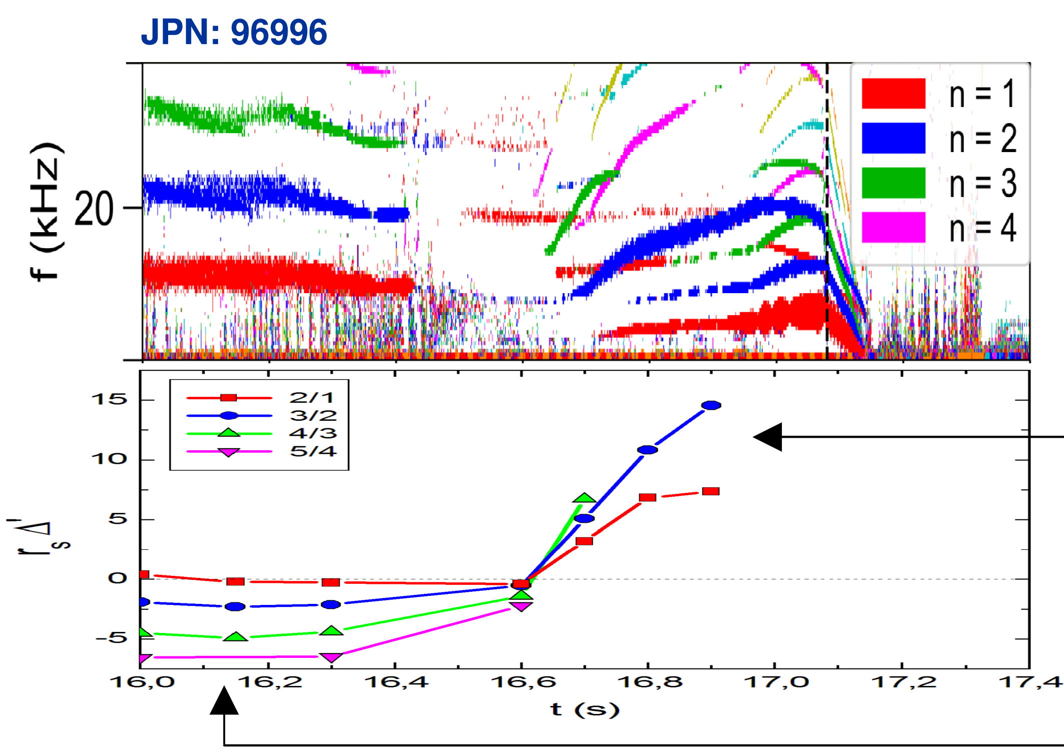

Linear stability analysis
(zero pressure limit)

$$\frac{d}{dr}\left[\left\langle\frac{g_{\theta\theta}}{\sqrt{g}}\right\rangle\frac{d}{dr}(rB_{r1})\right]=\left[\left\langle\frac{g_{rr}}{\sqrt{g}}\right\rangle m^2+\frac{\mu_0 q}{(1-nq/m)}\frac{d}{dr}\left\langle\frac{j_{tor}}{B_{tor}}\right\rangle\right](rB_{r1})$$

Field lines bending stabilizing term

Current density contribution

EC characteristic time scales

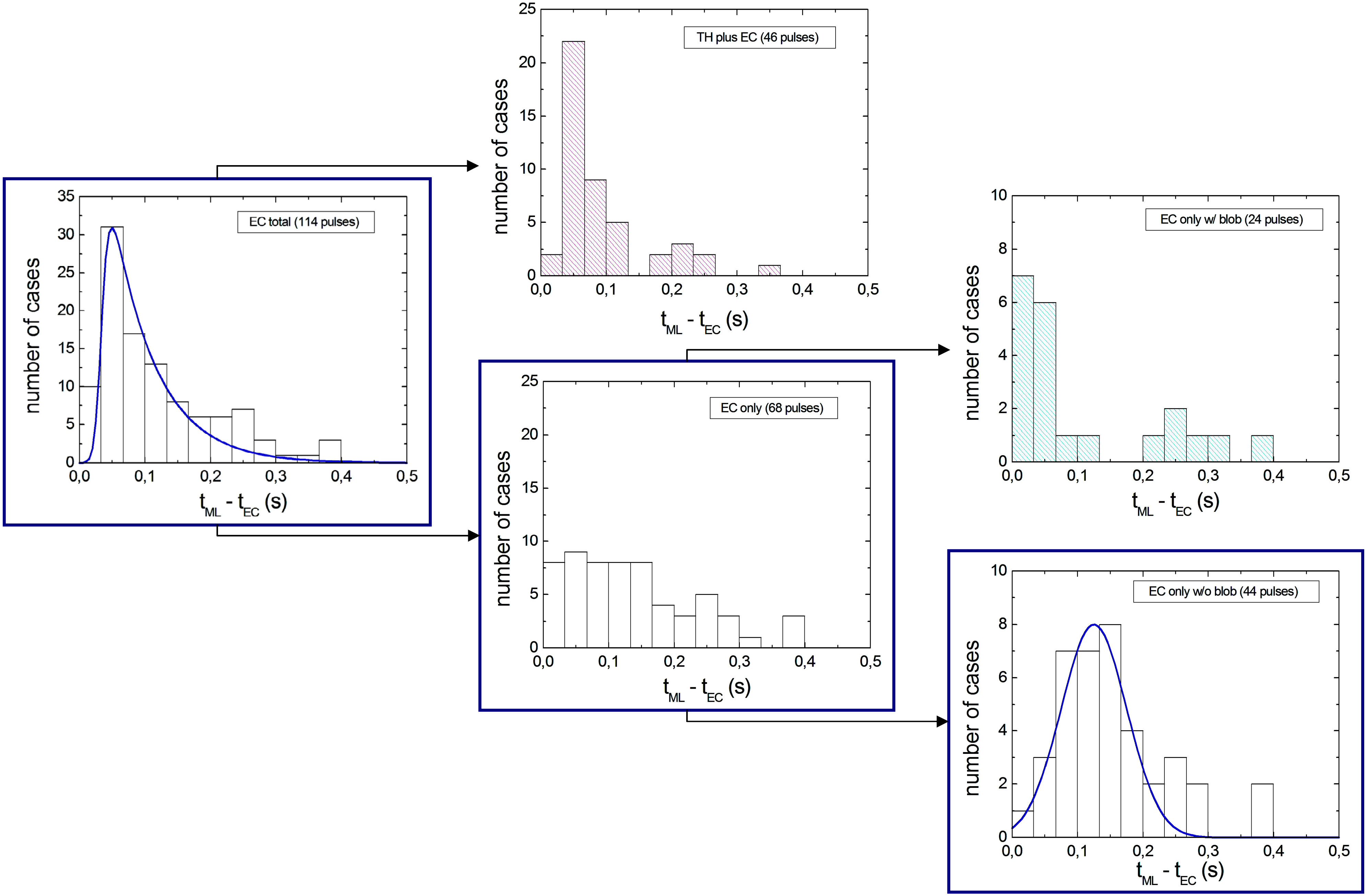

Outboard radiative blob

- An outboard radiating blob due to heavy impurities accumulated in the low field side can also lead to edge cooling and to the destabilization of a 2/1 TM, possibly locking and triggering the DMV intervention.

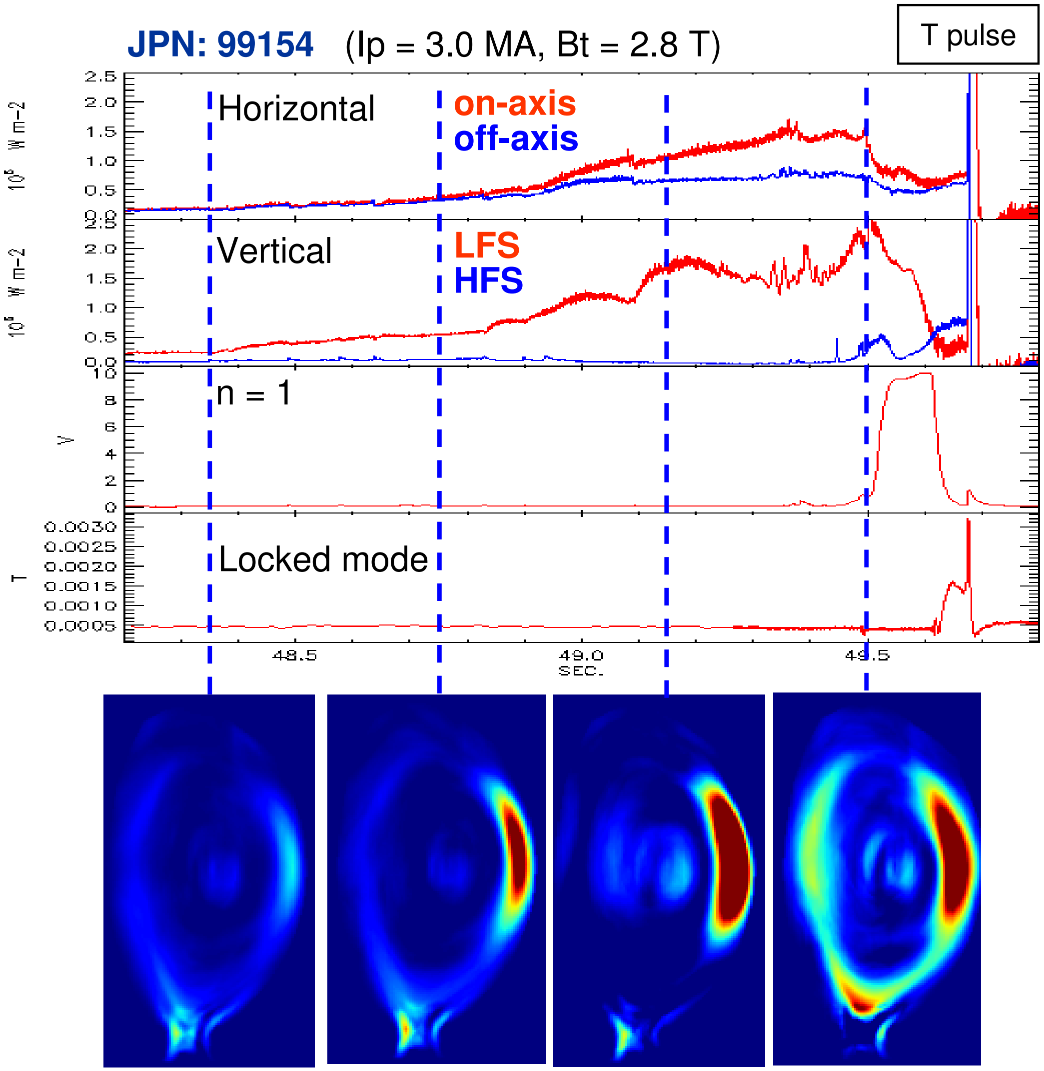

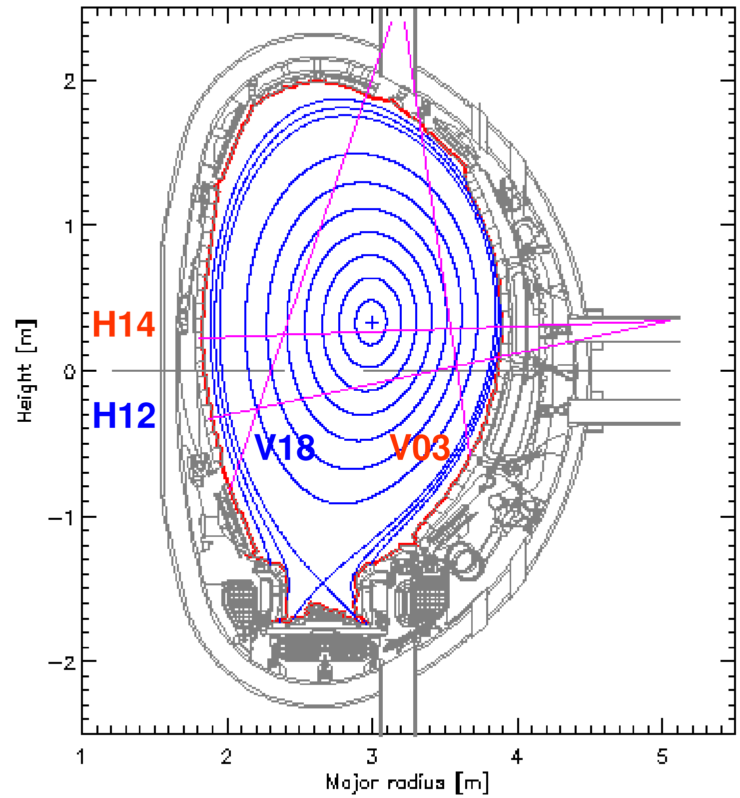

Signals from bolometer cameras:

Horizontal: BOLO/KB5H ch14, ch12
Vertical: BOLO/KB5V ch03, ch18

Synthetic diagnostics from bolometer data

- A "synthetic diagnostics“, based upon bolometer data, is developing to obtain radial profiles of radiation in a Z-band straddling the median plane, to be analyzed as done for the electron temperature profiles.

JPN: 96501

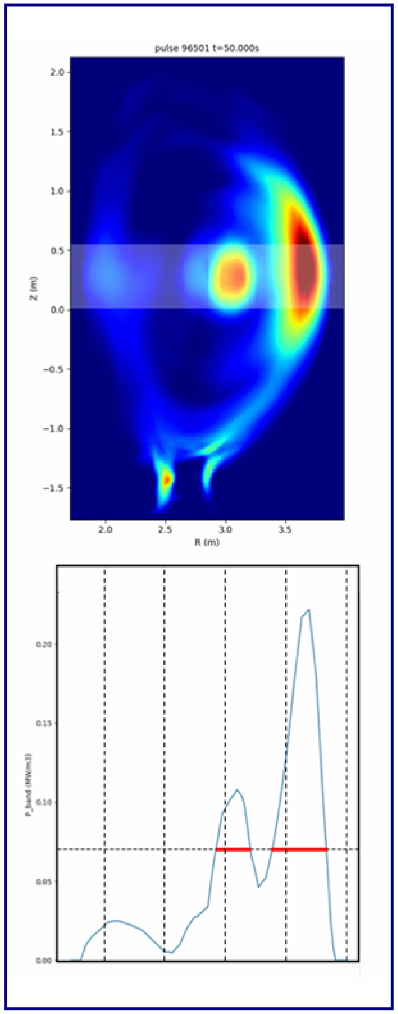

○ JPN: 92356

Contour levels (left) and radial profiles (right) of radiation in the Z-band straddling the median plane to highlight the transition from outboard blob to core accumulation. A final edge cooling is also present.

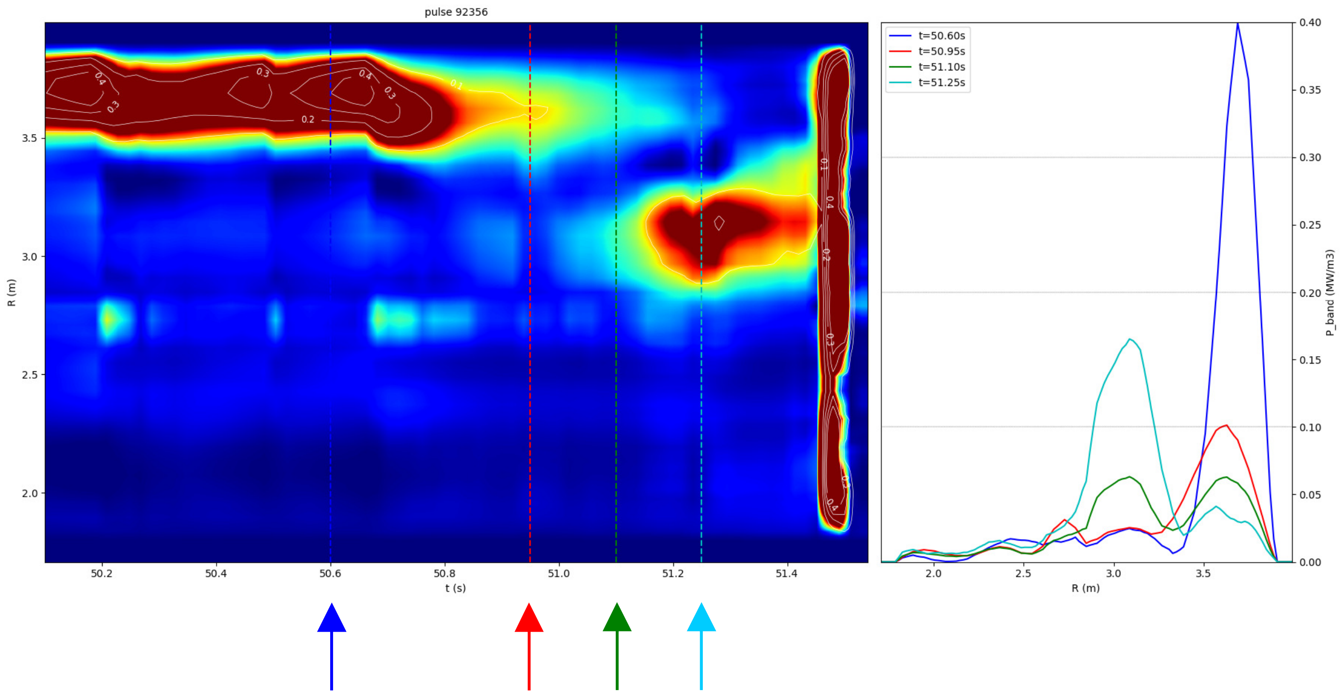

Disruption alerts from Te and radiation profiles

- The possibility of combining information on electron temperature (from ECE radiometry) and radiation profiles (from bolometer cameras) has been also considered.

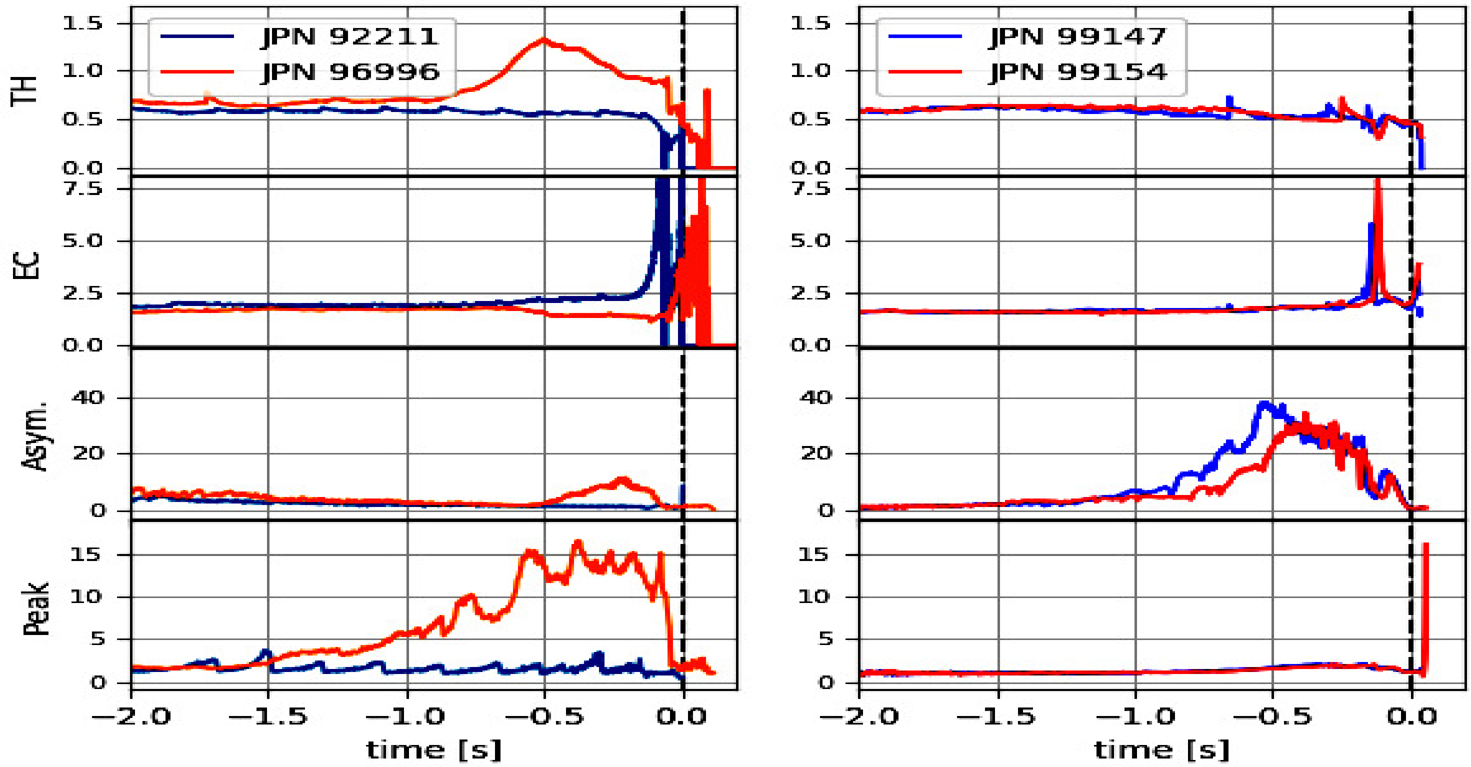

$$TH \equiv \frac{\langle Te \rangle_{Vmid}}{\langle Te \rangle_{Vint}}$$

$$EC \equiv \frac{\langle Te \rangle_{Vmid}}{\langle Te \rangle_{Vext}}$$

$$Asym \equiv \frac{VER_{LFS}}{VER_{HFS}}$$

$$Peak \equiv \frac{HOR_{on-axis}}{HOR_{off-axis}}$$

	Light impurities at the edge	Core impurity accumulation	Outboard radiative blob
Temperature Hollowing	- - -	AVOIDANCE	- - -
Edge Cooling	MITIGATION	- - -	MITIGATION
Radiation Asymmetry	- - -	- - -	AVOIDANCE
Radiation Peaking	- - -	AVOIDANCE	- - -

Termination panel

- In the Python Mode Analysis code for the study of MHD activity at JET, a panel dedicated to Termination has been introduced, providing inter-pulses information [E. Giovannozzi].

JPN: 99948 (Ip = 3.5 MA, Bt = 3.35 T)

DT pulse

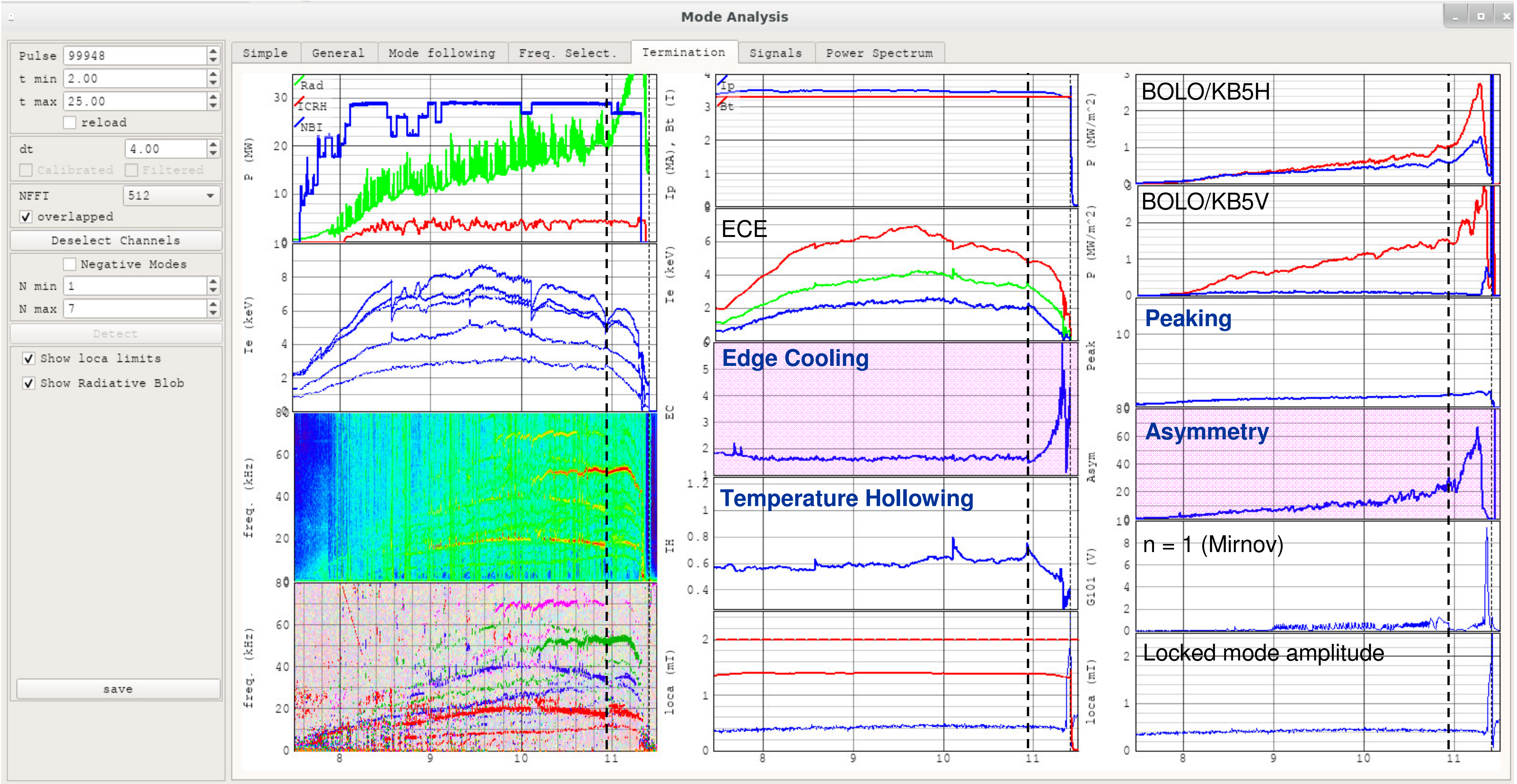

Locked modes and disruptions

- A widely adopted empirical criterion to trigger mitigation actions is based on the concept of a critical magnetic island size required to induce the thermal quench of a disruption.

$$w = 4\sqrt{\frac{r_s^2}{ms_s}\cdot\frac{B_{r1}(r_s)}{B_\theta(r_s)}} = 4\sqrt{\frac{ar_s}{nq_a s_s}\cdot\frac{B_{r1}(r_s)}{B_\theta(a)}}$$

$$q(r) = \frac{rB_T}{R_0 B_\theta(r)} \quad ; \quad s_s \equiv \left[\frac{r}{q(r)}\,\frac{dq(r)}{dr}\right]_{r_s} \quad ; \quad B_\theta(a) = \frac{I_p^{(MA)}}{5a}$$

Vacuum approximation $\quad r > r_s: \quad j(r) = 0 \;\Rightarrow\; I_p(r) = I_p \quad ; \quad q(r) \propto r^2$

$$\frac{B_{r1}(r_s)}{B_{r1}(r_c)} \approx f_B \cdot \left(\frac{r_c}{r_s}\right)^{m+1} \;\Rightarrow\; w = 4\sqrt{\frac{ar_c^{m+1}}{nq_a s_s r_s^m}\cdot f_B\,\frac{B_{r1}(r_c)}{B_\theta(a)}}$$

$$q(r) = \frac{2\pi B_T}{R_0\mu_0 I_p} r^2 \;\Rightarrow\; \frac{m/n}{q_a} = \frac{r_s^2}{a^2} \;\Rightarrow\; r_s = f_r \cdot a\sqrt{\frac{m}{nq_a}}$$

$$\frac{dq(r)}{dr} = \frac{2\pi B_T}{R_0\mu_0 I_p} 2r \;\Rightarrow\; s_s = 2\cdot f_s$$

$$m/n = 2/1: \quad \frac{w}{a} = 2\sqrt{\rho_c^3 \cdot \frac{f_B}{f_s f_r^2}\cdot\frac{B_{r1}(r_c)}{B_\theta(a)}}$$

l_i and q_a can be used to parameterize details of the *j*-profile wrt "vacuum approximation", through the variation of the three main factors:

$$B_{r1}(r_s)/B_{r1}(r_c), \quad r_s, \quad s_s$$

$$f_B = f_s = f_r = 1: \quad \left.\frac{B_{r1}(r_c)}{B_\theta(a)}\right|_{vac} = \frac{(w/a)^2}{4\rho_c^3}$$

The expected normalized levels for **ITER** baseline operation are estimated to be **5·10^-3^**, corresponding, for ρ_c = 1.32 to ***w/a* = 0.2**, which is a realist value.

$$\begin{cases} r_s \approx l_i^{0.30}/q_a^{0.64} \\ s_s \approx l_i^{0.80}/q_a^{0.64} \end{cases} \;\Rightarrow\; \left(\frac{w}{a}\right)^2 \propto \rho_c^3 \cdot \frac{q_a^{0.92}}{l_i^{1.40}}\cdot\frac{B_{r1}(r_c)}{B_\theta(a)} \approx \rho_c^3 \cdot \frac{q_a^{0.92}}{l_i^{1.40}}\cdot\frac{l_i^{1.20}}{q_a^{1.07}\rho_c^{2.9}} \approx \frac{\rho_c^{0.1}}{l_i^{0.2} q_a^{0.15}}$$

[P.C. de Vries Nucl. Fusion 2016]